



Master Thesis Applied Mathematics

Modelling of spontaneous glutamate plumes

Fleur van Alphen

May , 2023

Graduation committee

Dr. H.G.E. Meijer (Supervisor)
Prof. Dr. Ir. M.J.A.M. van Putten
Dr. M. Schlottbom

Faculty of Electrical Engineering,
Mathematics and Computer Science
Chair: Mathematics of Imaging & AI
University of Twente

1 Acknowledgements

I would like to express my sincere gratitude to my daily supervisor, Hil Meijer, for his unwavering support and encouragement throughout my research journey. I am truly grateful for his constant interest in my research, his insightful suggestions for new literature and experiments, and for always starting our meetings in a relaxed way by making conversation. It was always a pleasure to discuss my research progress with him.

I would also like to thank Michel van Putten for taking the time to discuss the research with me and giving me new insights into glutamate dynamics. His valuable feedback and suggestions have significantly contributed to the success of my research.

I am grateful to Matthias Schlottbom for accepting my invitation to join my exam committee and for reading my research thoroughly.

I would like to express my appreciation to Lilian Spijker for her generous support and willingness to offer a listening ear and think along on how to keep going. Without her guidance, I would not have been able to finish this research.

I would also like to extend my thanks to Ruben de Baaij for his constant support, encouragement, and motivation. His unwavering belief in me has been my driving force throughout my research journey.

Finally, I want to thank my family and friends for offering relaxation between researching and for being a listening ear during the ups and downs of my research journey. Their love and support have been a constant source of inspiration and motivation.

Contents

1	Acknowledgements	2
2	Introduction	5
3	Biological processes	7
3.1	Signalling in normal functioning neuron	7
3.2	Effect of energy deprivation	9
3.3	Glutamate plumes	10
3.3.1	In-vivo glutamate plumes in mice by Parker et al.	11
3.3.2	In-vitro glutamate plumes in brain slices by Ziebarth and Reiner	15
3.4	Occurrence of EAAT block	17
4	Computational Models with Glutamate Dynamics	17
4.1	Comparing candidate basis models	18
4.1.1	Reaction to OGD	19
4.1.2	Exchange with potassium bath	20
5	Methods	20
5.1	Modelling	20
5.1.1	Model implementation	22
5.1.2	Applied current	22
5.1.3	Energy deprivation	22
5.1.4	Varying neuronal glutamate transition rates	23
5.1.5	Calcium injection	23
5.1.6	Channel block	24
5.2	Motivation of simulations	24
6	Results	25
6.1	Glutamate release due to an applied current and energy deprivation	25
6.2	Impact of neuronal glutamate transition rates on glutamate release	28
6.3	Calcium induced glutamate release	29
6.4	Glutamate release due to temporal impairment of glutamate clearance	33
6.5	Cause of glutamate dip preceding glutamate peak	36
7	Discussion	40
7.1	Glutamate release due to applied current and ED	40
7.2	Impact of neuronal glutamate transition rates	40
7.3	Calcium induced glutamate release	40
7.4	Glutamate release due to temporal impairment of glutamate clearance	41
7.5	Cause of glutamate dip preceding glutamate peak	41

8	Limitations and further research	41
8.1	Limitations	41
8.2	Further research	42
9	Conclusion	43
A	Model formulation	49
A.1	Overview of the model notations	49
A.2	Neuronal dynamics	50
A.2.1	Voltage gated currents and leak currents	50
A.2.2	Active transport across neuronal membrane: NKA current	51
A.2.3	Secondary active transport across neuronal membrane: KCC	52
A.2.4	Secondary active transport: NCX	52
A.2.5	Secondary active transport: EAAT	52
A.3	Astrocytic dynamics	53
A.3.1	Kir4.1 channel	53
A.3.2	Secondary active transport: NKCC1	54
A.4	Glutamate cycle	54
A.5	Volume dynamics	55
A.6	Channel block	56
A.7	Model dynamics	56
A.8	Model constants and parameters	57
B	Adaptations to the model and the code from Kalia et al.	63
B.1	Calcium current in the code	63
B.2	Formula for GHK current	63
C	Proposal of additional glutamate cycle in the astrocyte	64
C.0.1	Specification of processes	64

Abstract

INTRODUCTION: In pathological conditions, glutamate release can show abnormal dynamic behaviour, characterized by plumes: a relatively large and fast increase in extracellular glutamate concentration, followed by a slow removal. Glutamate plumes appear to result from impaired astrocyte clearance of synaptically released glutamate. Although experiments with TTX show that plumes are independent of neuronal action potentials, the spontaneous activation of presynaptic voltage-gated calcium channels seems to be the source of the plumes.

OBJECTIVE: We aim to understand critical determinants of glutamate plume generation and clearance in silicon.

METHODS: We use an existing computational model of the tripartite synapse (Kalia PLoS Comput Biol. 2021) that includes extensive neuronal glutamate dynamics and energy-dependent dynamics. We aim to generate glutamate plumes in relation to ischemic stress, blocked channels, and as a response to various ion injections. We corrected several inconsistencies in the implementation, including the voltage-gated calcium current. We also analyze a flaw during the glutamate release that causes an implausible glutamate dip in the extracellular space before glutamate is released.

RESULTS: Our simulations indicate that energy deprivation may cause calcium-dependent synaptic glutamate release, independent of action potentials, but this glutamate release does not resemble glutamate plumes. We show that increased neuronal calcium concentrations alone are unlikely to cause noteworthy glutamate release, but calcium increase during a temporal astrocytic EAAT block can result in plume-like glutamate release. Furthermore, we show that even without neuronal glutamate release, a temporal astrocytic EAAT impairment can result in a plume-like extracellular glutamate transient.

CONCLUSION: Our research supports the hypothesis that a combination of impaired astrocytic EAAT and an increase in neuronal calcium can lead to glutamate plumes. We also propose that stochastic temporal astrocytic EAAT blocks could lead to glutamate plumes.

2 Introduction

More than 101 million people worldwide have experienced a stroke, and six and a half million people die from stroke annually [10]. During a stroke, a blockage in blood vessels causes a decrease in energy transportation to the brain [23, 49]. Under normal circumstances, the brain uses about 20% of the energy our body produces [33]. The energy shortage during a stroke can result in cognitive damage, paralysis, or chronic behavioural changes [34]. To better understand the mechanisms involved during a stroke, researchers try to understand the impact of energy deprivation on signal transmission.

An effect of energy deprivation is the release of neurotransmitters, which can result in deregulated neuronal signalling, cell death [44], and degradation of proteins [8]. Under normal circumstances, these neurotransmitters transfer signals between neurons. Excitatory signals mostly utilize the neurotransmitter glutamate. Energy deprivation can inhibit the transmission of ions through $\text{Na}^+\text{-K}^+\text{-ATPase}$, which disturbs ion dynamics and homeostasis. As a result, more glutamate can be released, while glutamate clearance is impaired [36, 12]. Buffers temporarily prevent harmful consequences, but the glutamate release may cause continuous signalling of one neuron to the next once buffers are full. The resulting excessive neurotransmitter concentrations can be fatal for signalling and the neuron.

In pathological conditions with impaired glutamate clearance, glutamate dynamics can show abnormal dynamic behaviour, which we call glutamate plumes. These plumes are characterized by a relatively fast increase in extracellular glutamate concentrations, followed by a slow removal, with a duration of typically 743 ± 620 ms and an amplitude similar to the amplitude during glutamate release after an action potential. These plumes are observed in-vivo in familiar hemiplegic migraine mice by Parker et al. [28], and in-vitro in rat slices by Ziebarth and Reiner [49]. The glutamate plumes most likely result from the spontaneous activation of voltage-gated calcium channels in combination with impaired astrocytic glutamate clearance. Parker et al. [28] hypothesize that stimuli that depolarize neural membranes, like a KCl injection and a spreading depression, are sufficient to induce plumes. This research investigates glutamate release after different stimuli to investigate which stimuli can trigger plume-like events.

Numerical models can help to investigate mechanisms underlying the glutamate plumes. Once a model exists, a single simulation is easily done without expensive techniques or long waiting times, as opposed to in-vivo or in-vitro experiments. Several biophysical models describe how ion gradients in neurons, glia, and surrounding areas change over time due to energy deprivation [18, 15, 9]. We will use the model by Kalia et al. [18] to answer the research question:

- What are possible causes for glutamate plumes?

To answer this question, we investigate two sub-questions:

- What is known about biological processes leading to neuronal and astrocytic glutamate release,
- Which adaptations to channel strengths, ion concentrations, or transition rates can induce glutamate release in the model, and is this glutamate release similar to glutamate plumes?

We hypothesize that circumstances similar to that of Ziebarth and Reiner [49] and Parker et al. [28] on itself will not generate glutamate plumes, but that a small calcium injection under these circumstances triggers glutamate release

similar to glutamate plumes. One would expect that a higher glutamate release rate causes extra glutamate release. We will check if this can be concluded from numerical experiments. We expect that experiments with inefficient glutamate clearance will give further insight into the mechanics of glutamate plumes.

We begin this paper by explaining the biological processes in the tripartite synapse, including signalling in a normally functioning neuron (section 3.1), the influence of energy deprivation on these processes (section 3.2), and the information we have on glutamate and glutamate plumes (section 3.3). Section 4 describes which model has been used, and how this model has been adapted to explore glutamate plumes. The analysis of the model and the results are described in section 6. Section 6.1 shows how an applied current and an energy deprivation can lead to glutamate release. A sensitivity analysis on forward rates in the glutamate cycle shows that the initial model is not likely to produce glutamate plumes (section 6.2). Section 6.3 investigates if a calcium injection under similar circumstances as experiments by Ziebarth and Reiner [49] and Parker et al. [28] can generate glutamate plumes. Section 6.4 investigates the effect of impairment of glutamate clearance through neuronal and astrocytic EEAT malfunctioning. Results show that even without neuronal glutamate release, a temporal astrocytic EAAT block induces an extracellular glutamate peak similar to the glutamate plumes. We aim to improve the model by investigating a shortcoming of the model, a glutamate dip, in section 6.5. Section 7 and 8 discuss the results and the limitations of this research and proposes further research. The conclusions can be found in section 9.

3 Biological processes

Before we can model glutamate plumes, it is important to understand the dynamics leading to normal glutamate release. Therefore, this section describes how signalling in a normal functioning neuron works. We will also describe the effect of energy deprivation since it is well-known that energy deprivation can result in glutamate release. Finally, we will summarize the main characteristics of glutamate plumes.

3.1 Signalling in normal functioning neuron

Neurons are fundamental parts of the brain that are responsible for processing all sensory input, determining what to do with this information, and sending commands to our muscles to react [46]. In this process, neurons communicate with each other by sending signals in the form of electrical pulses. Different compartments of neurons play a role in this signalling. A neuron consists of a soma, dendrites, and an axon which can be seen in Figure 1. Dendrites are branches of the soma that sense incoming signals and pass these on to the soma. If the signal is strong enough, the soma generates an action potential that propagates to the axon. The axon splits up and ends in several synapses. Dendrites

of other neurons are located near these synapses. Synapses have elaborate ion dynamics to pass the signal on to these dendrites. This research focuses on glutamate dynamics during signalling between synapses and dendrites.

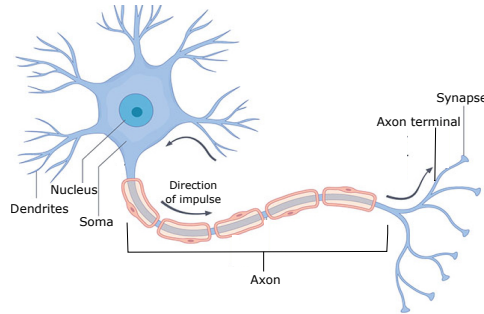


Figure 1: A neuron consists of dendrites, a soma, and an axon. The axon splits and ends up at synapses. An input is processed by the dendrites and propagates to the soma. Depending on the strength of the input, the soma generates an action potential or not. The action potential is sent through the axon to the synapses [27].

The signals sent from one neuron to the next consist of electrical pulses. Different ion concentrations inside and outside the cell cause a voltage on the cell membrane called the membrane potential. At a resting state, this membrane potential is approximately -70 mV and is called the resting potential. The physiological resting concentrations for different ions are regulated by a semipermeable membrane. When the neuron receives an excitatory stimulus, for example, an applied current, gates in the cell membrane open, allowing ions to flow along their gradient. The membrane potential increases, which is called depolarization. At the synapses, the current causes a release of neurotransmitters into the extracellular space by the presynaptic neuron, where they can activate receptors on the postsynaptic neuron to pass on the signal.

During signalling, different ions, gates, and currents are involved. Figure 2 shows the most influential processes. At rest, Na^+ and Cl^- concentrations are low in the neuron, causing an inward leak current, while the intracellular K^+ concentration is high and potassium leaks out of the neuron. These leak currents are relatively small. Specific ion gates open when a current is applied to the neuron, causing gated K^+ , Na^+ , and Cl^- currents. The neuron also contains some gates that can transport ions from low to high concentrations: The K^+-Cl^- -cotransporter uses K^+ to actively transport Cl^- out of the cell, and the Na^+/K^+ -ATPase (NKA) uses energy in the form of adenosine triphosphate (ATP) to transport Na^+ and K^+ against its gradient [18]. The NKA maintains the negative resting membrane by generating and maintaining the Na^+ and K^+ electrochemical gradients. This negative membrane potential is the basis for neuronal signalling, which makes NKA a crucial protein [26].

The synapse houses the presynaptic terminal, where Ca^{2+} and glutamate dynamics are crucial for synaptic transmission. At rest, Ca^{2+} concentrations are low and glutamate is stored in glutamate vesicles. When the membrane potential in the presynaptic terminal rises, the Ca^{2+} gates open, and Ca^{2+} concentrations in the presynaptic terminal rise. Glutamate vesicles bind to the neuronal membrane in a calcium-dependent process and release their glutamate into the cleft. Released glutamate can bind to postsynaptic receptors to pass the signal on to the postsynaptic neuron.

After the glutamate has been released, the neuron returns to its resting state. The neuron transports Ca^{2+} out of the cell with the Sodium Calcium Exchange protein (NCX) and takes up the released glutamate through an Excitatory Amino Acid Transporter (EAAT). However, neuronal glutamate clearance is relatively not fast and the EAAT does not return the other ion concentration to its resting state. Another cell type called astrocyte is located near the cleft. Its primary function is to buffer glutamate and ions, but the astrocyte also indirectly influences synaptic transmission. The excess glutamate in the cleft is cleared by a part of the astrocyte called the perisynaptic astrocyte process. The astrocyte maintains the extracellular ion concentrations, especially by removing K^+ ions that are released during an action potential. The clearance by the astrocyte allows the neuronal membrane potential to recover and prevents continuous signalling.

3.2 Effect of energy deprivation

Neurons need energy for several processes. Researchers suppose that the conservation of its structure, the creation of new proteins and lipids, and the traffic of organelles require high levels of ATP. However, the brain uses nearly 75% of its energy for signalling [citevergara2019energy,hofmeijer2012ischemic](#). The primary energy source of a neuron is ATP, a molecule made by ‘energy plants’ like mitochondria from glucose and oxygen. Blood vessels transport the glucose and oxygen to neuronal mitochondria to create the ATP molecules necessary in the brain [18].

A blood clot, blood leak, or another blockade in the blood vessel can decrease glucose transport and result in an energy shortage in the brain [45]. This energy deprivation deregulates processes and sometimes results in long-term and short-term problems. In the short term, changing ion concentrations deregulate neuronal signalling. Furthermore, cells swell, possibly irreversibly. The osmotic pressure becomes too high and may result in cell death.

The main consumer of ATP in the signalling process is NKA, which transports K^+ into the cell and Na^+ out of the cell [2]. The NKA pump is located in both neurons and astrocytes and normally helps to maintain a hyperpolarized rest-

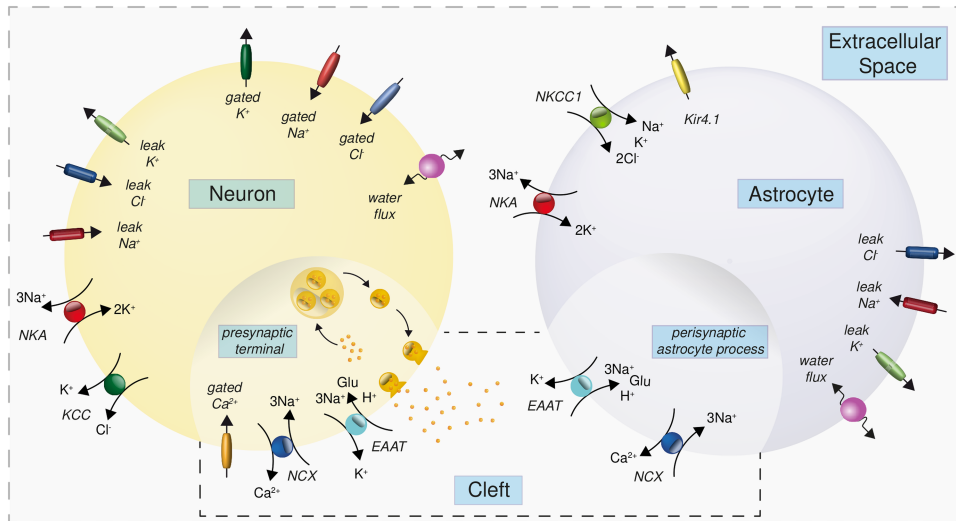


Figure 2: Active and passive transport of ions is regulated by different gates in the cell membrane of the neuron and the astrocyte. This image shows where the different gates are located and which currents they allow. Details can be found in section 3.1.

ing membrane potential. Low energy conditions reduce the NKA processes, and fewer K^+ and Na^+ ions can move against their gradient. K^+ ions accumulate in the ECS, while Na^+ concentrations in the cell are high [20, 13]. The changed ion concentrations depolarize the membrane potential. Voltage-dependent gates open, which deregulates the ion concentrations even more. Cl^- ions accumulate inside the cell and osmosis causes cell swelling or lysing: the breaking of the cell membrane. The high presynaptic Ca^{2+} levels result in continuous glutamate release into the cleft. The glutamate binds to postsynaptic receptors and causes excitotoxicity [4]. A wave of depolarization can spread from neuron to neuron, called spreading depolarization. When energy deprivation persists for a long period, these changes in ion concentrations can become irreversible. Cells break and cannot pass on signals anymore. This causes long-term problems that include paralysis and cognitive damage in the patient [14].

3.3 Glutamate plumes

Glutamate is an excitatory neurotransmitter that nerve cells use to send messages to other cells. The presynaptic terminal releases glutamate into the cleft to pass on a signal. In the cleft, it can bind to receptors on the membrane of post-synaptic cells to pass on the signal. Even though this process is essential for signalling in the brain, glutamate is also a toxic chemical that requires rapid removal from the cleft. If fast clearance fails, excessive activation of gluta-

mate receptors may excite nerve cells to death in a process called *excitotoxicity* [48, 3, 8]. In this process, the activation of glutamate receptors causes an excessive influx of sodium, chloride, and calcium. The resulting osmosis causes cell swelling until the cell bursts [44]. Furthermore, excessive calcium in the cell leads to the activation of enzymes that degrade proteins, membranes, and nucleic acids [8, 3].

When the neuron is at rest, glutamate is stored in vesicles in the neuron and the astrocyte. An action potential can lead to the opening of voltage-gated calcium gates, allowing canonical neuronal glutamate release, as described in section 3.1. However, glutamate can also be released spontaneously in a largely Ca^{2+} -independent manner. Furthermore, the spontaneous opening of voltage-gated Ca^{2+} channels can contribute a significant fraction of spontaneous release in excitatory synapses [35].

Both the neuron and the astrocyte contribute to the clearance of glutamate. The neuron transports the glutamate back to the presynaptic terminal through active transport by EAAT2 and EAAT5 proteins [24]. The astrocyte is the main absorber of glutamate and clears approximately 90% of the synaptically released glutamate [5, 7, 30]. The astrocyte uses EAAT1 and EAAT2 proteins to take up glutamate and glutamate enters vesicles in the astrocyte [24].

Both glutamate release and glutamate re-uptake can be affected by energy deprivation. Glutamate re-uptake is an ATP-dependent process and is reduced during energy deprivation [29]. Energy deprivation indirectly facilitates glutamate release through a wave of spikes [47]. These spikes occur after NKA deregulation, resulting in a depolarization of the membrane potential. The voltage-gated Ca^{2+} channels open to transport Ca^{2+} into the neuron, and these Ca^{2+} ions will cause glutamate release. After a short energy deprivation, ion concentrations will return to their original equilibrium. If energy deprivation persists for a long time, the shift of sodium and potassium concentrations may become irreversible. Glutamate concentrations in the neuron become lower while the extracellular glutamate concentration increase. This can lead to excitotoxicity [18].

3.3.1 In-vivo glutamate plumes in mice by Parker et al.

Recent research has found possible new consequences of impaired glutamate uptake on glutamate dynamics. In-vivo experiments have shown spontaneous plumes of released glutamate in mice with an FHM2 mutation (Figure 3). These mice have a GLT1a protein that works at 50% of normal capacity. The GLT1a is the mice equivalent of the human EAAT2 protein and is thought to be responsible for the majority of glutamate regulation [17, 31]. The amount of released glutamate during plumes was in the same order of magnitude as released glutamate during signalling. The duration of plumes was on average (\pm standard deviation) 743 ± 620 ms. The onset of the plumes is generally fast, while re-

covery is slow. Beside glutamate plumes, the mutation causes slow glutamate clearance from the synaptic cleft after sensory stimulation [28].

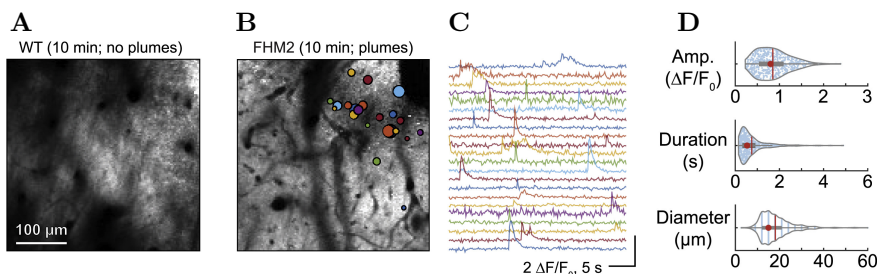


Figure 3: Average intensity projection from a wild-type (A) and an FHM2 (B) mouse with coloured circles overlaid to indicate the location and size of plumes. The wild-type mice generally do not show plumes under baseline conditions. Figure C shows the relative fluorescence amplitude of the FHM2 mice in Figure B ($\Delta F/F_0$). The FHM2 mouse shows 22 plumes in 10 minutes. Figure D shows the distribution of amplitude, duration, and diameter of 590 plumes from 7 FHM2 mice. The average amplitude of plumes is slightly lower than all other measured glutamate signalling, and the average (\pm standard deviation) duration was 743 ± 620 ms [28].

Many observed plumes in FHM2 mice last longer than 1 second. This suggests that glutamate clearance mechanisms malfunction during the plumes. To determine if the breakdown of glutamate clearance mechanisms directly causes the plumes, glutamate clearance was inhibited in normal mice with a glutamate transporter inhibitor (3S)-3-[[3-[[4-(Trifluoromethyl)benzoyl]amino]phenyl]methoxy]-L-aspartic acid (TFB-TBOA, short TBOA). This is a blocker that affects glial glutamate transport through EAAT1 and EAAT2 but does not affect EAAT4 and EAAT5. These wild-type mice showed a high frequency of plumes, while glutamate plumes were rare in wild-type mice without TBOA. These experiments show that the glutamate plumes are a consequence of impaired glutamate uptake. The frequency and diameter of TBOA-induced plumes were greater than those observed for spontaneous events in FHM2, which implies that TBOA impairs glutamate uptake even more than the FHM2 mutation [28].

Experiments with the voltage-gated Na^+ channel blocker tetrodotoxin (TTX) have shown that the plumes do not depend on neuronal action potentials. When the Na^+ channels were blocked for 30 minutes, no significant change was observed in the frequency, diameter, duration, or amplitude of the spontaneous plumes.

Since calcium plays a big role in glutamate release mechanisms, Parker et al. have tested the influence of calcium influx with the voltage-gated calcium blocker

Ni^{2+} . This causes a halving of the plume frequency, which implies that Ca^{2+} influx influences the plumes. Another experiment shows that the removal of extracellular Ca^{2+} significantly reduces the number of TFB-TBOA-induced plumes, supporting this hypothesis. Inhibition of Ca^{2+} influx through the glutamate-gated NMDA receptors did not influence plume frequency, indicating that Ca^{2+} enters the cell via other channels [28].

To determine if glutamate plumes are caused by vesicular release, the filling of vesicles was blocked by bafilomycin A1. Half of the brain slices of FMH2 did not show plumes after treatment with bafilomycin A1 and the median plume frequency was reduced. Injection with both veratridine and Baifilomycin A1 significantly increases the incidence of plumes in FHM2 mice. Veratridine prevents the inactivation of voltage-gated sodium channels. The resulting influx of Na^+ leads to the increase of neuronal Ca^{2+} concentrations, which stimulates the release of glutamate into the cleft. This indicates that plumes are induced by synaptic release and that the plumes are calcium-dependent. The astrocyte is also capable of vesicular glutamate release in a calcium-dependent manner. Parker et al. manipulated an astrocyte of FMH2 mice to see if astrocytic glutamate release could cause glutamate plumes. Mechanical stimulation and depolarizing current injections caused a response in Ca^{2+} but did not induce glutamate plumes. Therefore we hypothesize that glutamate plumes are induced by neuronal processes.

Since glutamate plumes seem to be induced by Ca^{2+} dependent synaptic glutamate release, Parker et al also examine the neuronal Ca^{2+} transients. When measuring presynaptic and postsynaptic Ca^{2+} FHM2 mice show plume-like Ca^{2+} events that originated from a central location and increased in size over time (Ca^{2+} plumes). To only measure presynaptic Ca^{2+} , the postsynaptic Ca^{2+} due to glutamate receptor activation is inhibited by a cocktail of glutamate receptor antagonists. The Ca^{2+} response was reduced by $\pm 56\%$, leaving a residual Ca^{2+} response that was presumably comprised of mostly presynaptic neural signalling. These same mice under influence of glutamate receptor inhibitors showed Ca^{2+} plumes, both with and without plume inducers (veratridine and thapsigargin). This suggests that at least a part of the Ca^{2+} plumes is presynaptic and that Ca^{2+} plumes do not require glutamate receptors. These findings support the hypothesis that plumes are the result of Ca^{2+} -dependent neuronal vesicular glutamate release.

Parker et al. also investigated the possible relevance of glutamate plumes in the onset of spreading depolarization. An injection of veratridine can initiate SD (both in-vivo and in-vitro), but veratridine is also a glutamate plume inducer. Increasing concentrations of veratridine increased both plume frequency and plume amplitude. When veratridine concentrations were high enough, the location of the plume became the origin of SD. The rise of plume frequency started at lower concentrations of veratridine in FHM2 mice than in wild-type mice, and less veratridine was necessary to induce an SD in FHM2 compared to FHM2

mice. However, similar plume frequencies and mean glutamate concentrations were observed just before the SD onset in FHM2 and wild-type mice. These results indicate that plumes are a form of glutamate dysregulation that occurs when a network approaches SD. It also implies that the threshold for SD onset does not depend on genotype and that differences in plume frequency between FHM2 and wild-type mice occur because of the rate at which the glutamate threshold is achieved. Interestingly, one mouse from each genotype did not have an increase in plume frequency before SD, which suggests that a rise in plume frequency is not necessarily required for veratridine-induced SD.

Inhibition of voltage-gated calcium gates by Ni^{2+} inhibits the incidence of plumes in most mice and eliminates the rise in glutamate concentrations. Ni^{2+} increased the SD threshold for veratridine by more than 3-fold and prevented SD onset in 4 out of 6 mice after a veratridine dose $< 750 \mu\text{M}$ and in 2 out of 6 mice with a dose $< 3 \mu\text{M}$. These results reinforce the hypothesis that the voltage-gated calcium channel is crucial for calcium-dependent glutamate release in veratridine-induced SD in FHM2 mice. It also suggests that additional glutamate-independent mechanisms are involved in SD ignition at higher concentrations of veratridine.

To determine if the presence of glutamate plumes is a general phenomenon in SD induction, or only in veratridine-induced SD, an SD is also induced by KCl injection. Again, all mice showed an increase in plume frequency at the location of injection before the SD. Glutamate concentrations increased for less than 10 seconds and did not rise with increasing KCl concentrations, which is in contrast with veratridine injection. The results confirm the association of plumes with SD initiation but do not mean that glutamate plumes lead to SD.

To check if glutamate plumes lead to SD or result from the waves of an SD, Parker et al. [28] injected KCl and induced an SD that propagated several mm. Away from the injection location, plume frequency, and glutamate concentrations did not rise before the SD wavefront (both in wild-type and in FHM2 mice), but glutamate concentrations did rise at the wavefront. Plume frequency only increased after the wavefront, during depolarization. The occurrence of plumes resolved with the decay in basal glutamate, suggesting that plumes subsided as clearance mechanisms were able to buffer extracellular glutamate back to pre-SD levels. The plume frequency was similar in wild-type and FHM2 mice, but plumes persisted for a longer period in FHM2 mice. The diameter and duration of each plume were also larger in FHM2 mice than in wild-type mice, which suggests that astrocyte clearance influences plume characteristics. These experiments suggest that glutamate plumes follow the wavefront of an SD and that plumes subside when excessive glutamate is cleared from the extracellular space.

Parker et al.[28] have initiated a model for glutamate release during glutamate plumes, which is shown in Figure 4. From all experiments by Parker et al. [28], we observe the following characteristics of plumes that are relevant to our

research:

- In-vivo glutamate plumes have a duration of 743 ± 620 ms and have an amplitude similar to glutamate released during normal signalling. The onset is relatively fast, and recovery is relatively slow.
- Glutamate plumes occur in mice in-vivo due to a breakdown of glutamate clearance. The plume frequency and diameter probably increase relative to the impaired rate of glutamate clearance.
- Plumes seem to not depend on neuronal action potentials, as shown by the experiments with TTX.
- Absence of plumes after Ni^{2+} injection indicates that plumes are generated through Ca^{2+} influx after action-potential-independent opening of the neuronal voltage-gated Ca^{2+} channels. Ca^{2+} influx through NMDA receptors does not influence the plumes.
- Glutamate plumes seem to be induced by neuronal Ca^{2+} -dependent synaptic glutamate release.
- Neuronal Ca^{2+} plumes precede the glutamate plumes, with a duration of ± 3 seconds and amplitude similar to Ca^{2+} release in normal signalling.
- Glutamate receptors are not required to induce glutamate plumes.

3.3.2 In-vitro glutamate plumes in brain slices by Ziebarth and Reiner

Ziebarth and Reiner [49] have observed similar plumes as Parker et al., but during in-vitro experiments instead of in-vivo. They make a clear distinction between synchronous activity, where different locations on a neuronal slice show synchronous glutamate release, and between glutamate plumes. The glutamate plumes have significantly longer durations than synchronous glutamate release, with a mean half-width duration (\pm standard deviation) of 322 ± 192 ms. The onset (10-90%) of the plumes is fast (166 ± 153 ms), the recovery (90-10%) of the plumes is slow (537 ± 331 ms), and plume amplitude is comparable to the amplitude of synchronous release.

Ziebarth and Reiner have shown that applying TTX in vitro did not influence the plume frequency, duration, or amplitude. This experiment is in line with the TTX experiment of Parker et al. and indicates that the glutamate plumes do not depend on neuronal action potentials.

Blocking the glutamate clearance with TBOA increased the plume frequency 37-fold. The plume size increased by a factor of 1.3, while plume duration and amplitude were not significantly influenced. This result aligns with the TBOA experiment of Parker et al. and supports the hypothesis that a breakdown of glutamate clearance is responsible for the glutamate plumes.

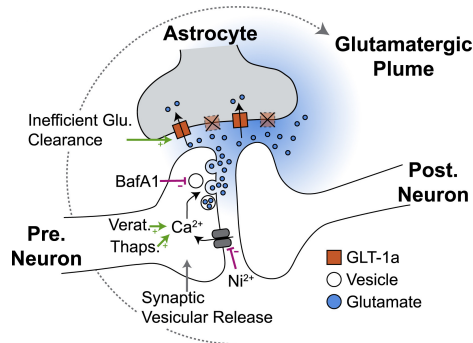


Figure 4: Glutamate release during plumes is likely due to Ca^{2+} -mediated vesicular release from neurons, as compounds that inhibit release (Ni^{2+} and BafA1) reduce the frequency of plumes (pink lines), whereas those that promote the release (veratridine and thapsigargin) increase the frequency of plumes (green arrows). Once glutamate is released, the presence of plumes is gated by impaired or inefficient glutamate clearance by astrocytes. Stimuli that depolarize neural membranes (KCl and SD) are sufficient to induce plumes. This model illustrates glutamate release from a single synapse for clarity, although release from multiple synapses may contribute to a single plume [28].

During chemical ischemia, plume frequency increases, plume duration doubles, and plume size increases by 50 %. Glutamate plumes appear to drive extracellular glutamate accumulation. Simultaneously, the spontaneous synchronized activity no longer occurs during the chemical ischemia. This experiment indicates that chemical ischemia alters neuronal or astrocytic processes responsible for plumes. It is not exactly clear which processes are involved in plume generation.

We summarize the experiments by Ziebarth and Reiner as follows.

- In vitro glutamate plumes have a half-width duration of 322 ± 192 ms, with a rise from 10% to 90% in 166 ± 153 ms and a decay from 90% to 10% in of 537 ± 331 ms.
- Experiments with TTX show that glutamate plumes do not depend on neuronal action potentials.
- Application of TBOA leads to more plumes indicating that a breakdown of glutamate clearance is responsible for glutamate plumes.
- Chemical ischemia influences processes that can generate glutamate plumes, but the experiment has not shown which processes are relevant.

3.4 Occurrence of EAAT block

Experiments by Parker et al. [28] show that glutamate plumes are an indicator for dysregulated glutamate clearance. The main glutamate clearance mechanism in neurons and astrocytes is the EAAT anion channel. The EAAT proteins, located on the neuron and the astrocyte, transport glutamate, Na^+ , and H^+ into the cell in exchange for K^+ . The most likely reasons for the disruption of glutamate clearance are a (partial) astrocytic EAAT block and/or a (partial) neuronal EAAT block. This section summarizes the literature on EAAT dysregulation.

Studies on Alzheimer's diseased brains have observed a permanent decrease in EAAT2 expression. [22]. This EAAT2 protein is mainly located on astrocytes, but can also be found on neurons. The EAAT2 protein is responsible for more than 90 % of glutamate uptake throughout the brain [19]. It is still unknown what causes the loss of function of EAAT2. Researchers hypothesize that the EAAT2 proteins may experience oxidative damage, resulting in loss of function. Furthermore, a cholesterol reduction in the membrane can lead to a loss of function of EAAT2 proteins. [22].

The same EAAT2 protein has a 30-95% loss of function in approximately 60-70% of Lou Gehrig's Disease (ALS) patients. Studies have found that EAAT2 expression in animals changes when exposed to symptoms of Parkinson's disease. The underlying mechanisms for this different expression of EAAT2 are still unclear. Researchers also found that overexpression of EAAT2 reduces excessive glutamate, helps to reduce epileptic attacks and helps to recover from a stroke [22].

For our research, we have not found incidences of natural short-term EAAT dysfunctionality. However, EAAT proteins can be blocked artificially by inhibitors dihydrokainic acid, TFB-TBOA, and dl-TBOA [37]. These EAAT blockers are not naturally produced by the body and therefore seem unlikely to be responsible for glutamate plumes.

4 Computational Models with Glutamate Dynamics

This research will use mathematical modelling to investigate the possible causes of glutamate plumes in a neuron. Since glutamate plumes are most likely released through synaptic calcium-dependent glutamate release, the model should contain neuronal calcium dynamics and calcium-dependent glutamate release. Experiments by Parker et al. [28] indicate that plumes are generated through Ca^{2+} influx after the opening of neuronal voltage-gated Ca^{2+} channels, so our model should contain this voltage-gated Ca^{2+} channel. Furthermore, the model has to contain glutamate clearance mechanisms that can be (partially) blocked,

since plumes occur due to a breakdown of glutamate clearance. To check if non-canonical glutamate release can be the cause of glutamate plumes, the model needs a mechanism to manually open voltage-gated calcium channels, or another method to simulate the stochastic inflow of calcium into the neuron.

After considering two candidate models ([18, 15]), we have determined to use the model of Kalia et al. [18] as a basis for this research. Section 4.1 shows the difference between the two models and substantiates our choice. The model equations are given in appendix A.

4.1 Comparing candidate basis models

Both Hubel et al. [15] and Kalia et al. [18] have created two different mathematical models to describe ion dynamics in a neuron, astrocyte, and extracellular space. Hubel et al. focus their numerical experiments on spreading depolarization caused by K^+ perfusion and oxygen-glucose-deprivation (OGD) in a model that includes a potassium bath. Kalia et al. focus on the change in the resting state of a neuron after energy deprivation, and the brain's ability to recover from energy deprivation. The models use different methods to determine the ion dynamics, and therefore similar experiments can show different results. This section will highlight the modelling differences and determines their influences on the simulations. For readability, we will call the model by Hubel et al. 'model H', and the model by Kalia et al. 'model K'.

One of the main differences between the two models is the modelling of glutamate release. Model K describes a full glutamate cycle in the neuron, such that the amount of released glutamate is proportional to the amount of calcium in the cell. This means that glutamate release is continuous over time and that without calcium, no glutamate is released. Model H omits the influence of calcium on glutamate release and assumes that glutamate is released at one moment when a threshold of the membrane potential is reached. Above this threshold, glutamate release is proportionate to the membrane potential and proportionate to the amount of available glutamate in the neuron.

Another difference between the models is the interpretation of the neuron. Model H utilizes a local average of glutamate concentration. Every synapse is assumed to connect to two neurons. Therefore only 50% of released glutamate will enter the ECS related to the modelled neuron. On the other hand, model K models a single neuron with its dynamics, and assumes all ions remain in the modelled tripartite synapse.

Also, the interaction with the surrounding of the neurons is different in the two models. Model K assumes all ions, all glutamate, and all water is confined to the modelled tripartite synapse. Model H assumes the neuron can exchange ions with a bath with a certain K^+ concentration. The diffusion of potassium ions with this bath enables the neuron's recovery and is responsible for a glutamate

peak at the end of the OGD. These results are shown in section 4.1.2

Furthermore, the dynamics of the ions are modelled differently. Model H does not model the calcium concentrations, does not include a K^+ - Cl^- -cotransporter or Na^+ - Ca^{2+} -transporter, and leaves out the voltage-gated Cl^- channel, as opposed to model K. Model H does include AMPA receptor gates and NMDA receptor gates for Na^+ and Cl^- , which are omitted in model K. Furthermore, model H includes cotransport of glutamate and chloride with a 1:1 ratio. Still, it is unclear which kind of gate allows for this transport.

One last difference is the modelling of the OGD. Model H assumes that the EAAT current is zero during the OGD, and therefore multiplies the EAAT current without OGD by the intensity of the OGD, to calculate the actual EAAT current. Model K does not assume direct consequences of the OGD to the EAAT current, but uses the ion concentrations to model the intensity of the EAAT current. EAAT transports one glutamate ion together with three sodium ions into the cell, in exchange for one potassium ion. During the OGD, the intracellular sodium concentration rises and the extracellular sodium concentration drops a lot so the EAAT current works against the diffusion of sodium ions. This causes the EAAT current to drop to almost 0. Therefore, the net EAAT current during OGD is almost similar in model H and model K, and we have not found significant changes due to this difference in simulations. The reaction to an OGD of both model H and model K are described in section 4.1.1.

After considering all these differences, we choose to use model K as our starting model. This decision is mainly based on the difference in the calcium cycle and in the modelling of the EAAT current. Model H entirely leaves out all calcium dynamics, while experiments by Parker et al.[28] show that glutamate plumes are generated through synaptic calcium-dependent glutamate release. Model K includes neuronal Ca^{2+} dynamics and, therefore, can mimic the glutamate release mechanisms of the experiments better. Since experiments have shown that a malfunctioning EAAT current can cause glutamate plumes, we also prefer a model for the EAAT current that is as accurate as possible. One advantage of choosing model H would have been the exchange of potassium ions with a K^+ -bath. This exchange is also present in the experiments of Ziebarth and Reiner. Furthermore, our simulation has shown that this exchange can cause glutamate peaks during recovery, which may be relevant to explain glutamate plumes. Potassium exchange to the bath in model K will not be present in this research but can be a useful topic of further research.

4.1.1 Reaction to OGD

Both model H and model K have experimented with oxygen-glucose deprivation (OGD). An OGD causes a series of spikes at the beginning of OGD in both models, but the rest of the reaction to energy shortage is different in the models. Own simulations in Figure 5aa show that model H can recover after any OGD,

however long it is. The system first seems to reach a new equilibrium, but this state is not actually an equilibrium. The same behaviour can be observed in model K during an energy deprivation of 15 seconds when setting $\alpha = 0.8$, the pump strength to 200 % (Figure 5ab). However, lowering the pump strength in model H does not prevent recovery, so another characteristic of model H must cause this difference. Simulations in section 4.1.2 show that the diffusion with the K^+ bath in model H causes this recovery. When this diffusion is set to 0, a new equilibrium can be reached and recovery depends on the length of the OGD, similarly as in model K. Model K can converge to a new equilibrium after an OGD, from where the system cannot recover to its original state. Figure 5b shows such a new equilibrium.

During the OGD, the membrane potential, the Na^+ concentration, and the K^+ concentration react similarly in both models. The chloride concentration in model H barely changes during the OGD compared to that in model K. This is due to the difference in chloride current: model H calculates this as the sum of leak current and cotransport current with potassium (KCC), while model K also takes the gated Cl^- -current into account. The extracellular glucose concentration behaves in the same manner in the two models, although the scale is different. Model K does not monitor the glutamate in the cleft.

The volume of the neuron and astrocyte increases in both models, although the volume in model H increases slower. Cell swelling is dependent on water permeability and chloride and sodium concentrations. Since chloride concentrations change little in model H, we would also suspect cell swelling to occur slower.

4.1.2 Exchange with potassium bath

The exchange of potassium with its surroundings in model H influences the recovery after an OGD of a neuron. Figure 6 shows that potassium exchange enables recovery of the neuron after a long OGD. During the OGD, neuronal potassium concentrations drop while extracellular concentrations rise. Without potassium exchange with a bath, the gates cannot transport ions fast enough to recover the neuron to its resting state. Exchange with a potassium bath removes excessive extracellular potassium ions and enables recovery. Before potassium concentrations in the neuron rise, they first decrease slightly, presumably because of diffusion with the ECS that now contains low concentrations of potassium. The potassium dip causes an increase in membrane potential, and therefore a peak in glutamate release occurs at this moment.

5 Methods

5.1 Modelling

This research simulates different situations using the model by Kalia et al. [18]. The general equations can be found in appendix A. The equations that are

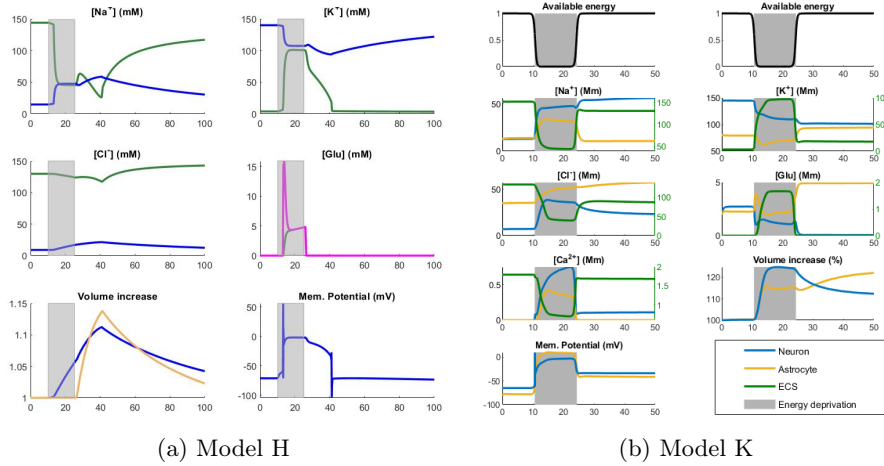


Figure 5: Shown is the reaction of OGD on the membrane potential and ion concentrations as modelled by Hubel et al. (left) and by Kalia et al. (right). Blue represents the intracellular space, green is the extracellular space, orange is the glia, and pink is the cleft. In model K we choose parameters $\alpha_0=0.2$, $t_{start}=10$, $t_{end}=25$, and $perc=0$. Results are described in section 4.1.1

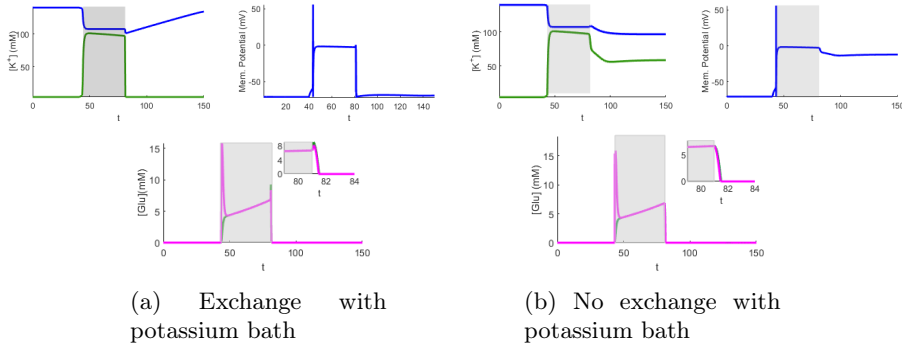


Figure 6: Shown is the effect of OGD with and without potassium exchange in model H. We show glutamate concentrations in the extracellular space (green) and in the cleft (pink), potassium concentrations in the neuron (blue) and ECS (green), and the membrane potential of the neuron. The grey area represents the duration of a 100% OGD. Exchange with a potassium bath (left) causes a peak of released glutamate during the OGD. The exchange with the potassium bath enables full recovery of the neuron after an OGD to resting states.

modified in some simulations will be described in this section. All modelling choices are also explained in this section.

5.1.1 Model implementation

We will solve the differential equations of the model by Kalia et al. [18] in MATLAB, using ode15s with a relative tolerance of 1e-10, absolute tolerance of 1e-10, initial step size of 1e-12 and max step size of 1e-4.

5.1.2 Applied current

In several experiments, we will apply a current in the form of a sodium injection to the system. This sodium injection depends on the timestep and is calculated as

$$I_{applied} = \left(1 - \frac{1}{1 + e^{\beta \cdot (t-t_0)}} + \frac{1}{1 + e^{-\beta \cdot (t-t_T)}}\right) \frac{A}{2F} \left(1 - \text{square}\left(\frac{2\pi(t+2.1)(1-\text{duty})}{\lambda/60}, \text{duty}\right)\right), \quad (1)$$

where t is the time (min), t_0 is the onset of the applied current (min), t_T is the offset of the applied current (min), β is the steepness of the applied current onset and offset, A is the amperage of the applied current (pA), F is Faraday's constant, and λ is the wavelength. $\text{Square}(\tau, \text{duty})$ is the function for a square wave with period 2π for the elements of the time array t . It is similar to the sine function but creates a square wave with values of -1 and 1 , where duty represents the percentage of the signal period in which the square wave is positive.

At the end of each timestep, the sodium is injected into the neuron by setting

$$N_{\text{Na}}^n = N_{\text{Na}}^n + I_{applied}, \quad (2)$$

where N_{Na}^i is the molar amount of Na^+ in compartment i , where n represents the neuron. The molar amount of Na^+ in the extracellular space will be determined as

$$N_{\text{Na}}^e = \text{Na}^+_{tot} - N_{\text{Na}}^n - N_{\text{Na}}^a \quad (3)$$

to assure the conservation of ions in the system. Here, e represents the extracellular space, and a represents the astrocyte. Na^+_{tot} is the total amount of Na^+ in the system.

5.1.3 Energy deprivation

When a shortage of ATP is available in the tripartite synapse, we speak of energy deprivation (ED). We simulate energy deprivation by temporarily blocking and subsequently restoring the NKA current in the neuronal and astrocyte compartment. The NKA current is given by

$$I_{\text{NKA}}^n(t) = \left(\frac{I_{\text{NKA}}^{max}(t)}{100}\right) P_{\text{NKA}}^{scale} P_{\text{NKA}}^n g_{\text{NKA}} \frac{[\text{Na}^+]_n^{1.5}}{[\text{Na}^+]_n^{1.5} + (\alpha_{\text{NKA}}^n)^{1.5}} \frac{[\text{K}^+]_e}{[\text{K}^+]_e + (\beta_{\text{NKA}}^n)}, \quad (4)$$

details about this current can be found in section A.2.2. The function $I_{\text{NKA}}^{\text{max}}$ is used to simulate energy deprivation for some time and is defined as

$$I_{\text{NKA}}^{\text{max}} = P_{\text{min}} + (1 - P_{\text{min}})I_{\text{block}} \quad (5)$$

$$(6)$$

where

$$I_{\text{block}}(t) = (1 + \exp(\beta(t - t_1)))^{-1} + (1 + \exp(-\beta(t - t_2)))^{-1}. \quad (7)$$

The start and end time t_{start} and t_{end} of the ED can be chosen freely and determines the values of t_1 and t_2 by

$$t_1 = t_{\text{start}} - \frac{1}{\beta} \log(1/P_{\text{min}} - 1), \quad (8)$$

$$t_2 = t_{\text{end}} + \frac{1}{\beta} \log(1/P_{\text{min}} - 1). \quad (9)$$

The parameter β represents the steepness, and P_{min} is the minimum available energy when the ED is induced.

5.1.4 Varying neuronal glutamate transition rates

In section 6.2 we vary the neuronal glutamate transition rates. We adapt the reaction rates one by one to see their influence on the simulations. When we change these rates, we make sure to not change the leak currents to investigate only the influence of the reaction rates.

5.1.5 Calcium injection

We model a calcium injection similarly to the sodium injection in section 5.1.2. The amount of injected calcium on time t is calculated as

$$\text{Ca}^{2+}_{\text{applied}} = \left(1 - \frac{1}{1 + e^{\beta \cdot (t - t_0)}} + \frac{1}{1 + e^{-\beta \cdot (t - t_T)}}\right) \frac{A}{2F} \left(1 - \text{square}\left(\frac{2\pi(t + 2.1)(1 - \text{duty})}{\lambda/60}, \text{duty}\right)\right), \quad (10)$$

where t is the time (min), t_0 is the start time of the calcium injection (min), t_T is the end time of the calcium injection (min), β is the steepness of the onset and offset, A is the intensity of the calcium injection, F is Faraday's constant, and λ is the wavelength. $\text{Square}(\tau, \text{duty})$ is the function for a square wave with period 2π for the elements of the time array t , with duty cycle duty .

For a neuronal calcium injection, we update the molar amount of neuronal calcium to

$$N_{\text{Ca}}^{\text{n}} = N_{\text{Ca}}^{\text{n}} + I_{\text{applied}}. \quad (11)$$

For an astrocytic calcium injection, we update the astrocytic molar amount of calcium to

$$N_{\text{Ca}}^a = N_{\text{Ca}}^a + I_{\text{applied}}. \quad (12)$$

The molar amount of Ca^{2+} in the extracellular space will be determined as

$$N_{\text{Ca}}^e = \text{Ca}^{2+}_{\text{tot}} - N_{\text{Ca}}^n - N_{\text{Ca}}^a \quad (13)$$

to assure the conservation of ions in the system. Here, N_{Ca}^e represents the molar amount of Ca^{2+} in the extracellular space, and $\text{Ca}^{2+}_{\text{tot}}$ is the total amount of Ca^{2+} in the system.

5.1.6 Channel block

The flux through normal functioning channels is described in appendix A.2 and A.3. In several simulations, we block the neuronal EAAT current, the astrocytic EAAT current, and the NKA current. These channel blocks all function in a similar method, where we multiply the normal flux through the channel by the functionality of the channel:

$$J_{\text{blocked channel}} = J_{\text{functioning channel}} \cdot \text{channel functionality}. \quad (14)$$

Here, $J_{\text{blocked channel}}$ is the flux through the channel during the block, and $J_{\text{functioning channel}}$ is the flux through an unblocked channel, for which equations can be found in appendix A.2 and A.3. The channel functionality is calculated as

$$\text{channel functionality} = \mu + (1 - \mu) \cdot \left(\frac{1}{(1 + e^{\beta_1 \cdot (t-t_0)})} \cdot \frac{1}{(1 + e^{\beta_2 \cdot (t-t_T)})} \right), \quad (15)$$

where μ is the minimum functionality of the channel as a number between 0 and 1. t_0 and t_T denote the beginning and end time of the channel block (min). β_1 and β_2 represent the steepness of the onset and offset of the channel block.

5.2 Motivation of simulations

We will perform several simulations to investigate which stimuli and which types of stress can trigger plume-like glutamate release.

We first simulate glutamate release due to an applied current, to observe if glutamate release in our model functions properly. Since glutamate plumes have a similar amplitude as glutamate release induced by an action potential, this simulation also gives us insight into the amplitude a glutamate plume in our model should have.

We also stimulate glutamate release after energy deprivation. Experiments of Ziebarth and Reiner [49] show that glutamate plumes become more frequent and have a longer duration when chemical ischemia is induced. The simulation can show what happens to glutamate concentrations during energy deprivation and may give insight into why plumes become more pronounced. Furthermore, changes in ion concentrations and glutamate clearance can give insight into which processes are relevant for glutamate plumes, and which are not.

Since glutamate plumes are probably induced by neuronal calcium-dependent vesicular release, we also investigate the impact of neuronal glutamate transition rates on glutamate release. The model contains an extensive glutamate cycle in the presynaptic terminal, including neuronal calcium-dependent glutamate release. We expect that altering the transition rates influences the glutamate release after an applied current or during energy deprivation. such a change may give insight into the mechanisms behind glutamate plumes.

Furthermore, we want to simulate the neuronal calcium-dependent vesicular release under similar circumstances as Parker et al. [28] and Ziebarth et al. [49]. To mimic the tripartite synapse of an FHM2 mouse, we use a 50% functional astrocytic EAAT and a 50% functional NKA. We hope that a calcium injection in the neuron under these circumstances can generate action-potential independent plume-like glutamate release. Furthermore, we also inject calcium in the astrocyte, to see if the astrocyte would be able to release glutamate similar to the neuron. To ensure that glutamate release is action-potential independent, we block the voltage-gated sodium channel in the simulation.

Glutamate plumes occur due to a breakdown of glutamate clearance. Therefore we simulate a long-term and a short-term astrocytic EAAT block. We hope the glutamate release during this block gives insight into the glutamate plumes.

To conclude, we conduct experiments on the functionality of our model. We have observed a flaw in our model, which results in an extracellular glutamate dip where one would expect a rise in extracellular glutamate levels. Since this flaw prevents the comparison of characteristics of glutamate release in our model to the characteristics of glutamate plumes, we advise solving this flaw in further research. We show glutamate concentrations in all different stages, and we experiment with EAAT strength, to find the cause of this glutamate dip.

6 Results

6.1 Glutamate release due to an applied current and energy deprivation

Research [18, 42] shows that both an applied current and an energy deprivation can be responsible for neuronal glutamate release. Fig 7 shows the impact of an

applied current and energy deprivation on ion concentrations and glutamate release in our model. An applied current in the form of a neuronal Na^+ injection induces neuronal action potentials and depolarizes the astrocyte. The depolarization opens the voltage-gated calcium channels, shortly increasing calcium conductance and causing a large increase in neuronal calcium. The neuronal calcium increase triggers the docking of synaptic vesicles, resulting in neuronal glutamate release. The amplitude of released glutamate is $4.6 \cdot 10^{-5}$ mM/L. When stimulation stops, the membrane potential and ion concentrations return to baseline. During energy deprivation, the NKA is dysfunctional, allowing Na^+ ions to accumulate in the neuron and astrocyte and retaining K^+ ions in the extracellular space. The change in charges depolarizes the neuron and astrocyte, allowing Ca^{2+} to enter both cells via voltage-gated calcium channels and enabling neuronal glutamate release. The shifted Na^+ and K^+ balance decreases both neuronal and astrocytic EAAT functionality, which slows down the re-uptake of glutamate by the neuron and astrocyte. During the energy deprivation, a total of $3.3 \cdot 10^{-3}$ mM/L glutamate is released into the cleft.

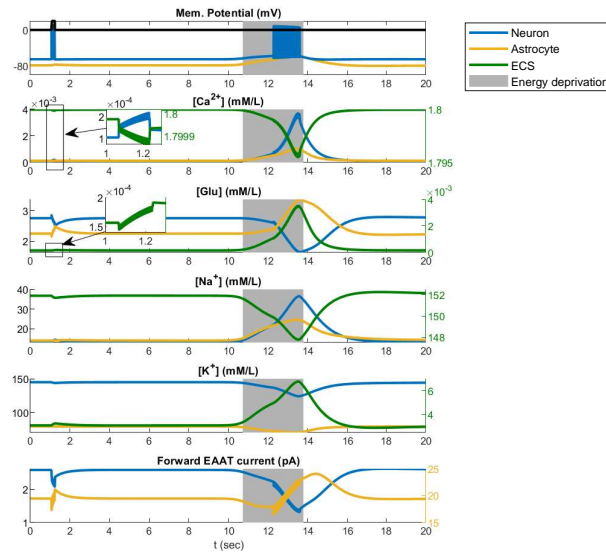


Figure 7: Time courses of the membrane potential and sodium, potassium, calcium, and glutamate concentrations in response to a current pulse (20 pA, 5 min, black trace) and in response to an energy deprivation (50% energy, 5 min, gray area). The stimulus causes action potentials, which trigger Ca^{2+} inflow into the neuron. The neuronal Ca^{2+} enables glutamate release into the cleft. Astrocytic and neuronal EAAT proteins remove the glutamate from the cleft. Due to ED, the neuron depolarizes leading to a wave of action potentials. The depolarization enables Ca^{2+} inflow into the neuron, triggering neuronal glutamate release.

We simulate a short energy deprivation of one second, both with and without

a blocked gated Na^+ current, to investigate the influence of glutamate release through action potentials (Figure 8). With a normal functioning voltage-gated Na^+ current, energy deprivation results in a wave of action potentials, and each action potential is responsible for a new burst of incoming Ca^{2+} , resulting in a burst of glutamate release. A short dip in extracellular glutamate precedes every increase in extracellular glutamate, which is expected to be a shortcoming of the model, explained in section 6.5. When the voltage-gated Na^+ is blocked, the neuron depolarizes but does not show a burst of action potentials. The depolarization still allows the inflow of Ca^{2+} into the neuron, and calcium-dependent glutamate release is observed. The two simulations show comparable amounts of released glutamate, indicating that glutamate release due to energy deprivation is mostly independent of action potentials. The duration of glutamate increase is approximately 1 second, and recovery takes approximately 1 minute (not shown in figures), while in-vitro plumes have an onset of approximately 170 ms and decay of 530 ms.

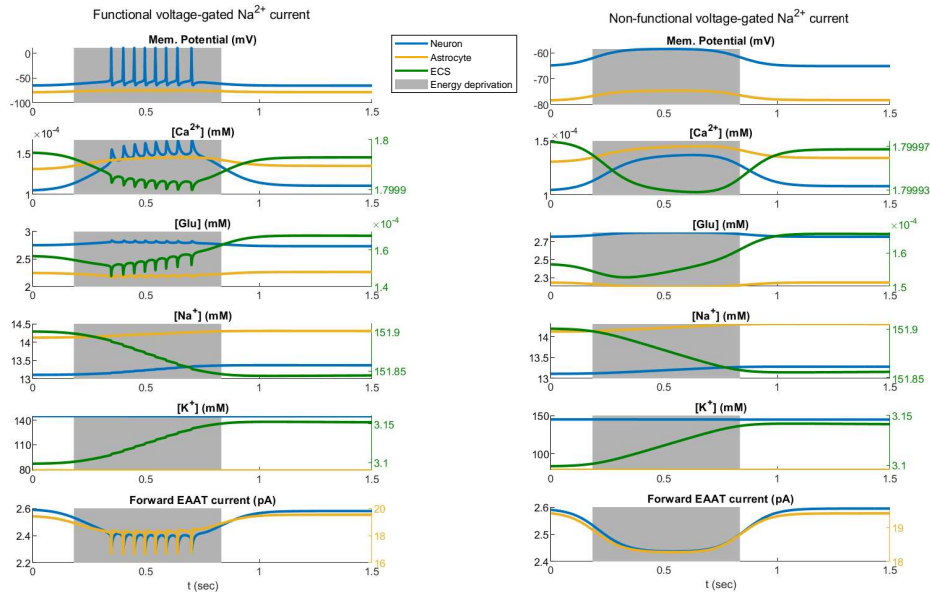


Figure 8: Energy deprivation during 1 second indirectly results in calcium-dependent glutamate release. Under normal circumstances, glutamate is released after action potentials (left), but suppression of action potentials by a voltage-gated Na^+ block (right) barely affects the total amount of glutamate released. The duration of the glutamate peak is significantly longer than that of glutamate plumes, while the amplitude of extracellular glutamate is lower.

6.2 Impact of neuronal glutamate transition rates on glutamate release

Parker et al. have shown that glutamate plumes are probably induced through neuronal calcium-dependent glutamate release. Our model has an extensive glutamate cycle in the presynaptic terminal, including the neuronal calcium-dependent glutamate release. Figure 9 shows the different glutamate states and possible transitions between the states. We expect that altering the transition rates can influence the dynamics of glutamate release, and may give insight into the mechanisms behind glutamate plumes. Therefore we will apply a sensitivity analysis to the glutamate cycle in the tripartite synapse. A sensitivity analysis generally determines how target variables are affected based on changes in input variables. In our case, we investigate how glutamate release is affected by changes in transition rates. We adapt the reaction rates one by one to see their influence on the simulations.

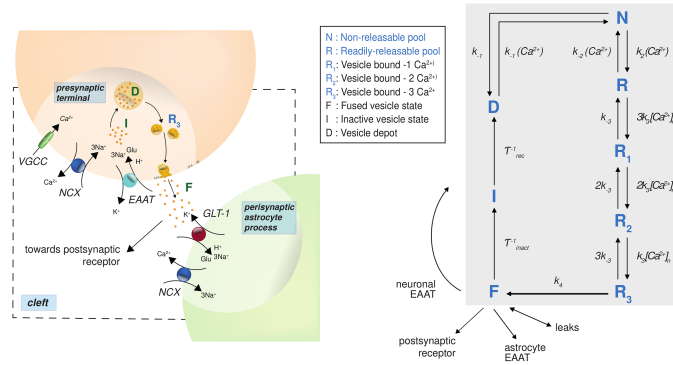


Figure 9: Glutamate recycling scheme in the presynaptic terminal described by Kalia et al. [18]. (Left) schematic view of the different glutamate states and ion dynamics at the presynaptic terminal. (Right) the various transitions between the different glutamate states.

The rate at which glutamate in a vesicle depot transforms to a non-releasable pool is represented by k_1 . It is a function of the maximum forward rate $k_{1,max}$ and the Ca^{2+} half-saturation concentration rate K_M :

$$k_1 = k_{1,max} \frac{[\text{Ca}^{2+}]_n}{[\text{Ca}^{2+}]_n + K_M}. \quad (16)$$

We vary k_1 by changing the parameter K_M . We predict that low values of k_1 cause fewer vesicles to be filled with glutamate, and so less glutamate can be released. Therefore more glutamate remains in the neuron and less glutamate will be found in the synaptic cleft. However, for values of K_M varying between 0.001 and 0.01, we did not see any notable differences in the simulation results

during an applied current or energy deprivation. A similar simulation is conducted as in Figure 7

The transitions from the non-releasable pool to the readily releasable pool and back are represented by k_2 and k_{-2} . These rates are functions of a forward rates k_{20} and k_{-20} respectively and of the Ca^{2+} half-saturation concentration rate K_{DV} :

$$k_2(\text{Ca}^{2+}) = k_{20} + g(\text{Ca}^{2+})k_{2cat} \quad (17)$$

$$k_{-2}(\text{Ca}^{2+}) = k_{-20} + g(\text{Ca}^{2+})k_{-2cat} \quad (18)$$

$$g(\text{Ca}^{2+}) = \frac{[\text{Ca}^{2+}]_n}{[\text{Ca}^{2+}]_n + K_{DV}} \quad (19)$$

We have adapted the parameter k_{DV} to analyse the effect of different calcium requirements for vesicles to become releasable. The experiments show that changing K_{DV} does not affect the results. A possible explanation for the unchanged results is a lack of noteworthy change in the net flow ($k_2 - k_{-2}$). To analyse the effect of changing the ratio between k_2 and k_{-2} we vary k_{-20} . We expect that a value of k_{-20} that is higher than k_{20} cause fewer vesicles to be readily releasable, such that glutamate release is very low. However, simulations with k_{-20} varying between $1\text{e-}5$ and $4\text{e-}5$ did not show notable differences.

The rate at which vesicles bind to the cell membrane is described by the parameter k_3 . Changing the value of k_3 between 1 and 10 did not have any effect on the results of the simulations. Varying the rate k_4 at which vesicles fuse with the cell membrane between 0.5 and 5 did not influence the glutamate release in our simulations.

6.3 Calcium induced glutamate release

Experiments by Parker et al. indicate that plumes are induced by calcium-dependent vesicular release. Since both neurons and astrocytes allow vesicular glutamate release, they have manipulated an astrocyte to see if an astrocyte could induce glutamate plumes. An increase in astrocytic Ca^{2+} was observed, but no plumes arose. Therefore, they hypothesize that neuronal processes induce plumes. We investigate the influence of a calcium injection in the neuron and the astrocyte and observe if such an injection can lead to glutamate plumes. We mimic the experiment settings from [28] and [49]. The experiments by Parker et al. [28] focus on the effect of the FHM2 mutation in mice in comparison to wild-type mice. They show that plumes do not occur in wild-type mice but arise in FHM2 mice with a mutation that reduces EAAT2 and NKA functionality by 50%. We mimic the in-vivo circumstances using a small extracellular space ($\alpha = 0.2$). To model the FHM2 mutation, we use a 50% functional astrocytic EAAT and a 50% functional NKA. We use a calcium injection of 2.5 seconds since Parker et al. measured a calcium increase before the glutamate plumes

lasting 2.5-3 seconds. The results can be seen in Figure 10a and 10b. The experiments from Ziebarth and Reiner [49] are conducted in an in-vitro situation. Glutamate plumes occurred under baseline conditions, but a blockade of the EAAT current by TBF-TOA increased plume frequency. We mimic the in-vitro situation using a large ECS ($\alpha = 0.8$) and simulate the effect of TBF-TOA by setting the EAAT current at 50% functionality. In addition, we use an NKA current with 50% functionality for comparability with the in-vivo experiments. Again, we use a calcium injection of 2.5 seconds. These simulations are shown in Figures 10c and 10d. Both Parker and Ziebarth have shown that plumes are not affected by a blockade of Na^+ -gates by TTX and are thus not induced by neuron action potentials. We block the gated Na^+ -current in all experiments to ensure that the glutamate increase is not induced by action potentials but solely by a calcium increase.

The different circumstances all result in different baselines. The EAAT currents in the FHM2 simulations are functioning at 50% of their capacitance, so we expect the EAAT current in the FHM2 simulation to be lower than the EAAT currents in the wild-type simulations. This hypothesis is correct for the astrocytic EAAT current, but the neuronal EAAT current in the FHM2 simulation is higher than that of the simulation corresponding to wild-type mice. We hypothesize that the low-functioning astrocytic EAAT current causes lower extracellular K^+ concentrations and higher extracellular Na^+ and glutamate concentrations, which amplifies the neuronal EAAT current. The in-vivo and in-vitro simulations also have different baselines. The total Na^+ concentration in-vitro is higher than the total amount of Na^+ in-vivo since the extracellular space is bigger in-vitro. The neuronal EAAT current is higher in-vitro than in-vivo.

In all simulations, we apply a current to the neuron in the form of a Na^+ injection around $t = 5$. By conservation laws, extracellular Na^+ concentrations decrease, which slightly depolarizes the neuronal membrane. The K^+ gates open, and the rising extracellular K^+ concentrations inhibit the EAAT currents. Usually, the depolarization would augment the gated Na^+ current, but this current is blocked in the simulation. Therefore the membrane potential cannot depolarize further, and the neuron does not fire action potentials. The depolarization opens the neuronal Ca^{2+} gates and the rising Ca^{2+} concentrations trigger neuronal glutamate release. The weaker EAAT and NKA currents in the FHM2 simulation cause a higher glutamate peak than the wild-type situation, presumably because of the slower uptake of glutamate. The larger ECS of the in-vitro simulations causes a lower increase in glutamate concentration.

Around $t = 20$, we inject a Ca^{2+} current into the neuron, and around $t = 37$ we inject Ca^{2+} into the astrocyte. The injected Ca^{2+} enables glutamate release in both cases, but excessive amounts of Ca^{2+} are needed to induce a glutamate peak as high as the peak during the applied current: An injection of 1 mM Ca^{2+} enables a glutamate peak that is smaller than the peak after a Ca^{2+} increase

of $3 \cdot 10^{-5}$ after an applied current. To investigate why so much calcium is needed to generate glutamate release, we simulated normal calcium injections of $\pm 3 \cdot 10^{-5}$ mM Ca^{2+} in Figure 11. For these small Ca^{2+} injections, glutamate concentrations barely rise. During the applied current, the neuronal and astrocytic EAAT currents are weaker because of the decreasing extracellular Na^+ concentrations. This gives glutamate a chance to rise. Both the neuronal and astrocytic Ca^{2+} injection barely influence the Na^+ concentrations, so the neuronal and astrocytic EAAT currents remain at their normal strength. Therefore, all released glutamate is immediately taken up by the EAAT proteins and does not accumulate in the cleft.

All simulations show a glutamate decrease in the ECS before a glutamate increase occurs. This decrease is a modelling flaw: the neuron and astrocyte do not contain a glutamate buffer in the model, so the cell needs to contract glutamate out of the ECS before glutamate can be released. If we ignore this glutamate decrease, we see that the amount of glutamate released in wild-type is consequently lower than the glutamate released in FHM2 (see table 1). In vitro, this difference suggests that a calcium injection induces glutamate plumes in FHM2 mutations more often than in the wild-type. A higher plume frequency in FHM2 mice is in line with the increased plume frequency during TBOA experiments by Ziebarth and Reiner [49]. The difference in glutamate increase between wild type and FHM2 in-vivo is too small to make any conclusions. Furthermore, a calcium injection in the neuron results in a lower glutamate peak than an injection in the astrocyte in an in-vivo situation, while the reverse is true in an in-vitro situation.

Table 1: Glutamate increase after applied current and after neuronal or astrocytic Ca^{2+} injection in different situations, measured as the difference in maximal and minimal glutamate

	Wild-type	FHM2
Applied current in-vivo	$7.4 \cdot 10^{-6}$ mM/L	$9.8 \cdot 10^{-6}$ mM/L
Applied current in vitro	$5.8 \cdot 10^{-6}$ mM/L	$7.8 \cdot 10^{-6}$ mM/L
Neuron injection in-vivo	$1.0 \cdot 10^{-5}$ mM/L	$1.3 \cdot 10^{-5}$ mM/L
Neuron injection in-vitro	$6.2 \cdot 10^{-6}$ mM/L	$8.3 \cdot 10^{-6}$ mM/L
Astrocytic injection in-vivo	$1.5 \cdot 10^{-5}$ mM/L	$1.7 \cdot 10^{-5}$ mM/L
Astrocytic injection in-vitro	$4.4 \cdot 10^{-6}$ mM/L	$6.0 \cdot 10^{-6}$ mM/L

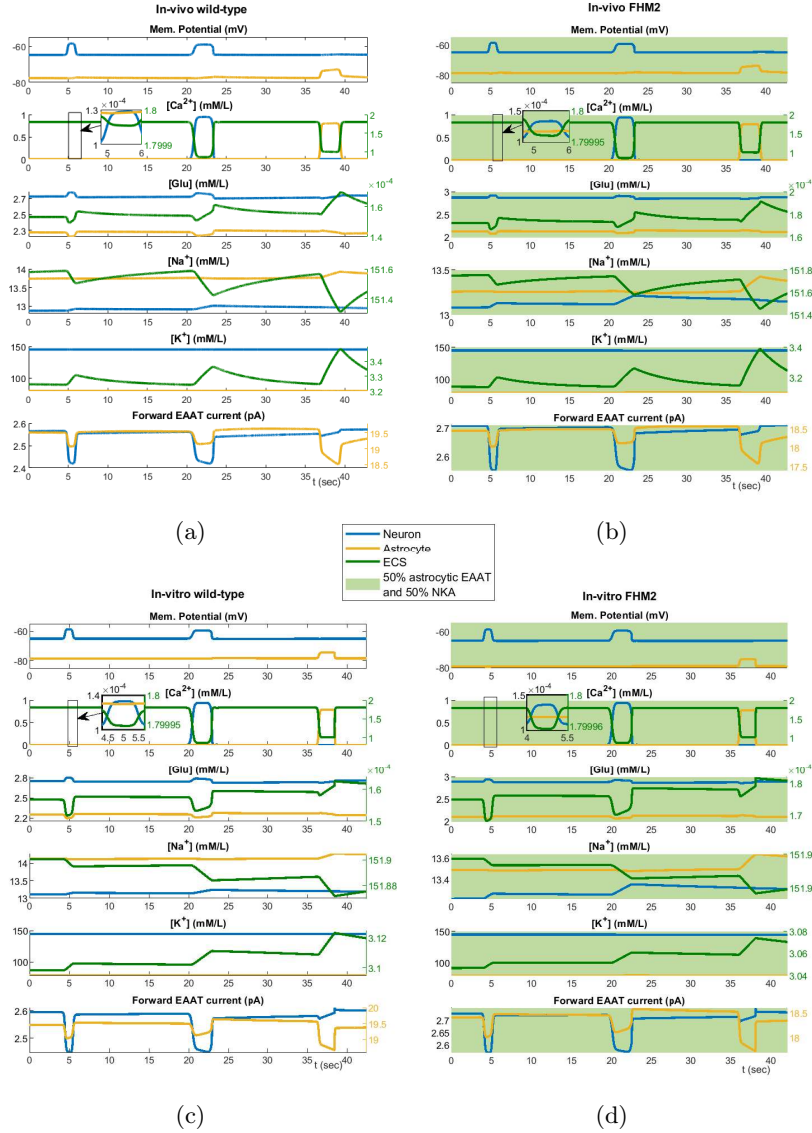


Figure 10: The effect of a calcium injection on the neuronal and astrocytic dynamics. around $t = 5$ we inject a current of 20 mV for 1 second. Around $t = 20$ we inject Ca^{2+} into the neuron for 2.5 seconds and around $t = 37$ we inject Ca^{2+} into the astrocyte. The upper figures use a small ECS ($\alpha = 0.2$) to imitate an in-vivo situation, while the lower figures use a big ECS ($\alpha = 0.8$) to match an in-vitro situation. The left figures show the simulation of wild-type (i.e. functional EAAT and NKA) and the right figures show a simulation of an FHM2 mutation (i.e. 50% functional astrocytic EAAT and NKA protein). All simulations have a blocked gated Na^+ current to prevent glutamate release due to action potentials.

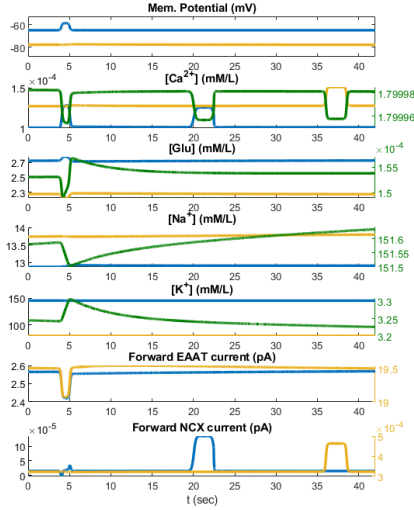


Figure 11: At $t=5$, an applied current causes a neuronal calcium increase, which enables glutamate release. At $t=20$, a neuronal calcium injection does not trigger a glutamate release. At $t=37$, an astrocytic calcium injection also does not enable a glutamate release. The simulation uses an extracellular space of 0.2 and the gated Na^+ current is blocked.

6.4 Glutamate release due to temporal impairment of glutamate clearance

Glutamate is cleared from the cleft by both neuronal and glial EAAT proteins. This section analyses the effect of blocking these EAAT currents. In-vitro experiments show that an astrocytic EAAT block with TBOA results in more glutamate plumes. We imitate this situation in a simulation with an astrocytic EAAT block. Since incomplete glutamate clearance is a hypothetical cause for glutamate plumes, we also simulate a neuronal EAAT block and a block of both neuronal and astrocytic EAAT.

The astrocytic EAAT protein is responsible for transporting glutamate, Na^+ , and H^+ into the astrocyte in exchange for K^+ . When the astrocytic EAAT block is initiated (Figure 12), this exchange is disrupted, causing an increase in extracellular glutamate and Na^+ concentrations, and a decrease in extracellular K^+ . This changes the neuronal Nernst potentials of Na^+ , K^+ , and glutamate, causing an increase in the neuronal EAAT current. The neuronal EAAT transports Na^+ and glutamate into the neuron in exchange for K^+ , increasing neuronal Na^+ and glutamate concentrations, and decreasing neuronal K^+ .

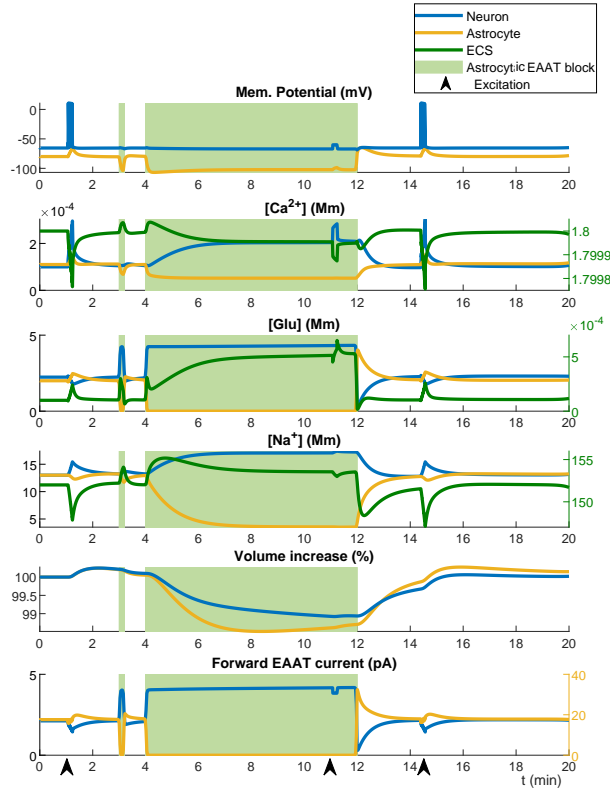


Figure 12: Simulation with current pulse at 20 mA at $t=1$ and $t=14.7$, and at 100 mA at $t=11$. The astrocytic EAAT is blocked at $t \in [3, 3.2]$ and $t \in [4, 12]$.

The change in the neuronal Nernst potential of K^+ influences the KCC current, which co-transport K^+ and Cl^- ions out of the neuron. During the decrease in extracellular K^+ , the KCC current increases, resulting in a decrease of neuronal Cl^- concentrations and an increase of extracellular Cl^- concentrations. The later decrease in neuronal K^+ reduces the KCC current, resulting in Cl^- accumulation in the neuron. The change in osmotic pressure gradient through Na^+ and K^+ approximately cancel each other out, while the Cl^- decrease reduces the osmotic pressure gradient in both the neuron and astrocyte, leading to a decrease in their volumes.

Under normal circumstances, an increase of neuronal Na^+ depolarizes the membrane potential and triggers an action potential. The depolarization also opens voltage-dependent Ca^{2+} gates, resulting in increased neuronal Ca^{2+} concentrations and enabling neuronal glutamate release. However, the onset of the astrocytic EAAT block only causes a slight depolarization of the neuronal membrane. This depolarization seems sufficient to trigger a significant inflow of Ca^{2+} and

initiate a neuronal glutamate release.

To further investigate the absence of an action potential during Na^+ increase during an astrocytic EAAT block, we applied a current to the neuron during the astrocytic EAAT block. The simulation shows that the depolarization due to the applied current is too small to initiate an action potential. This is caused by a shift in the Nernst equilibria of the different ions.

Typically, the increased membrane potential opens voltage-dependent Ca^{2+} gates to increase neuronal Ca^{2+} concentrations and enable neuronal glutamate release. In absence of action potentials, the small depolarization of the membrane potential after an applied current during an astrocytic EAAT block appears to be sufficient for such Ca^{2+} uptake. Only a small part of this calcium influx is facilitated by the gated calcium current ($3 \cdot 10^{-6}$) and by the Ca^{2+} leak current ($3 \cdot 10^{-5}$), the calcium increase is mainly caused by the NCX current ($1.6 \cdot 10^{-4}$). The Ca^{2+} increase is responsible for neuronal glutamate release.

The simulations with an astrocytic EAAT block show an increase of glutamate in the cleft due to insufficient clearance, while the glutamate peak is not induced by action potentials. The glutamate increase, therefore, shows relevant similarities to the observed glutamate plumes in [49, 28]. Biological experiments of [28] show that plumes have an average duration and standard deviation of 0.7 ± 0.6 seconds. The experiments in [49] show an average duration and standard deviation of 0.3 ± 0.2 seconds with an amplitude in the same order of magnitude as glutamate plumes that are induced by action potentials under normal circumstances. We try to create plume-like events with these characteristics by partially blocking the astrocytic EAAT current in different ways (Figure 13).

The first simulation in Figure 13 shows three successive astrocytic EAAT blocks of one second where the functionality of EAAT gradually decreases. The EAAT works at 0%, 10% and 50% per cent consecutively. The glutamate peaks that arise last one second. The amplitude of the peak at 0% functionality is in the same order of magnitude as glutamate peaks arising after an applied current. When EAAT has more functionality, the glutamate peaks become lower. The duration and amplitude of the glutamate peak during a 0% functional astrocytic EAAT block match the observed glutamate plumes of [28], but glutamate plumes arise very fast and resolve slowly, while the simulation shows a gradual rise and decrease of glutamate concentrations.

Our second simulation uses a more abrupt astrocytic EAAT block to account for the fast extracellular glutamate increase. This generates a glutamate peak that lasts 0.05 seconds. The onset time is fast, as expected, but the recovery phase is equally fast. Therefore these peaks do not resemble the observed glutamate plumes. Extracellular glutamate concentrations reach a concentration of 0.002 mM/L by a full block, 0.0003 mM/L when EAAT functionality is 10% and they barely increase for EAAT functionality of 50%. This means the full

EAAT block and the 50% functional EAAT block do not resemble the amplitude of glutamate plumes, but a 10% functional EAAT current results in an amplitude comparable to glutamate plumes. The duration of the glutamate peak is shorter than that observed in glutamate plumes. Another inconsistency with the glutamate plumes is that the extracellular glutamate concentration remains above the resting level until the EAAT block is lifted.

The third simulation uses a combination of a fast onset of the EAAT block, with a slow recovery of the EAAT current. The plumes in [49] have an average rising time of 166 milliseconds and an average recovery time of 536 milliseconds. We try to reproduce this result with our simulation by using an EAAT block of 700 milliseconds that reaches a full block after 166 milliseconds and recovers slowly in the next 534 milliseconds. We now see the same fast rise time and slow decay time as the data of the plumes in the paper of Ziebarth and Reiner [49]. The amplitude of the glutamate peak during a 0% functional EAAT resembles the amplitude of the glutamate plumes. Therefore, an abrupt EAAT block in the astrocyte with a slow recovery is a possible explanation for the glutamate plumes.

In the literature, we mainly found occurrences of EAAT2 blockades when looking for glutamate uptake impairment (see section 3.4). Furthermore, experiments by Ziebarth and Reiner [49] show that EAAT2 functionality influences plume frequency. We will also consider a combination of neuronal and astrocytic EAAT block in this research because EAAT2 can also be found on neurons. The simulation with both neuronal and astrocytic EAAT blocked shows higher and more abrupt peaks than a simulation with working neuronal EAAT proteins. A full block of all EAAT currents cannot be responsible for the glutamate plumes, since the peak is a lot higher than the glutamate peak after excitation. However, a block of 50 % of all EAAT currents can cause a peak with similar amplitude and duration as the observed glutamate plumes and can therefore be a plausible cause of the plumes.

6.5 Cause of glutamate dip preceding glutamate peak

All experiments with glutamate release show a dip in extracellular glutamate that precedes the extracellular glutamate increase. We cannot find a logical reason for glutamate to decrease before a glutamate plume occurs. Furthermore, in vitro and in vivo experiments do not show this glutamate dip. This suggests that the dip is caused by a shortcoming of the model, which can either be solved by parameter tuning or by adapting the equations of the model.

It is generally assumed that a healthy neuron contains a glutamate depot with sufficient glutamate [43]. Newly absorbed glutamate is stored in the depot. When a neuron needs to release glutamate, it utilizes the glutamate from the depot. Our model contains such a depot, but we hypothesize that the depot in our model is too small. Therefore, not all required glutamate can be extracted

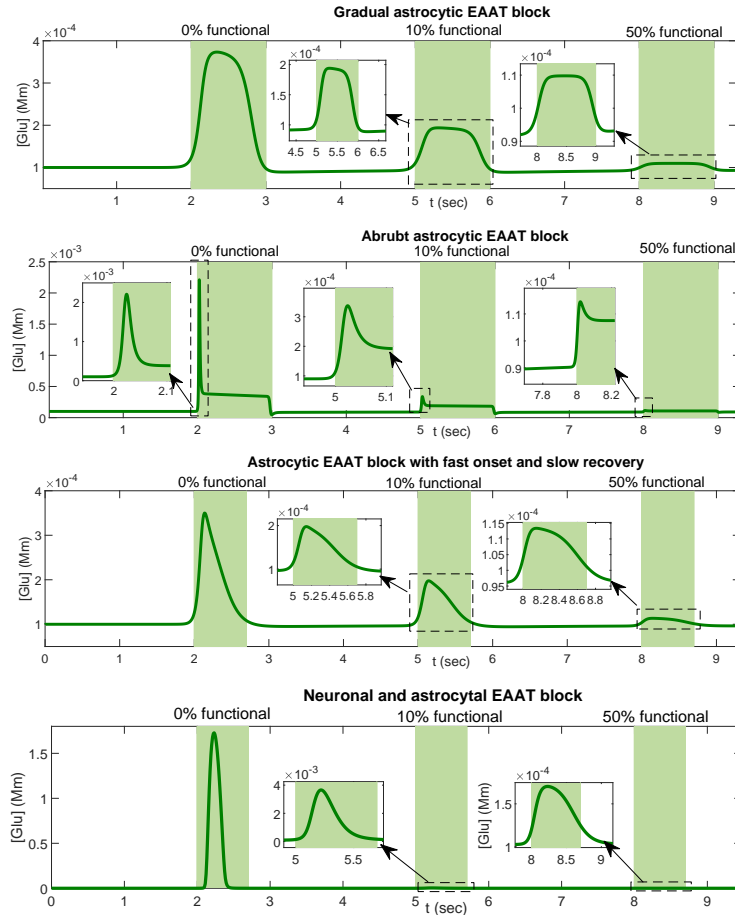


Figure 13: The extracellular glutamate concentration during different types of EAAT blocks. In each simulation, the first block fully blocks the EAAT channels. The EAAT channels can still function at 10 % of their normal capacitance during the second block and 50% during the third block.

from the depot, and glutamate needs to be extracted from the cleft before glutamate release is possible.

To test our hypothesis, we look at the amount of glutamate in different stages prior to glutamate release. We use a neuronal calcium injection together with a block of voltage-gated Na^+ channels to generate glutamate release. We use this particular induction of glutamate release because the simulations in Figure 10c with neuronal calcium injections show relatively high glutamate dips. Figure 14 shows the concentrations of glutamate in different stages. After a neuronal calcium injection, glutamate is transported from the cleft into the neuron, causing the glutamate dip in the cleft. Glutamate is released from the neuron into the cleft, causing the glutamate peak. In this process, the glutamate depot is almost empty and does not function. We expect that the glutamate dip would not occur if the glutamate depot contained a larger glutamate buffer at rest. Furthermore, if the glutamate uptake decreases, we expect the glutamate dip to be lower.

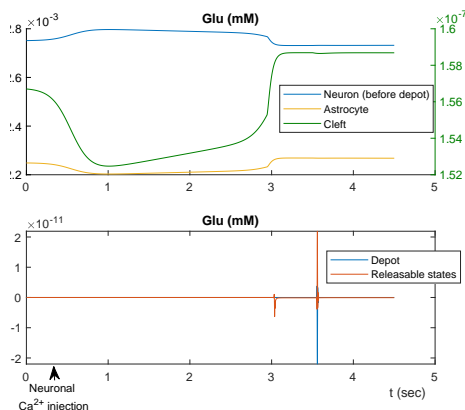


Figure 14: Glutamate dynamics after a neuronal calcium injection, where we differentiate between astrocytic glutamate, glutamate in the cleft (stage F), glutamate in the neuron before entering the depot (stage I), glutamate in the depot (stage D), and glutamate in releasable states (stages N, R, R_1 , R_2 and R_3). The simulation shows that a neuronal calcium injection initiates a glutamate dip in the cleft prior to the glutamate peak. This glutamate is first transported into the neuron, and later released back into the cleft. At rest, the depot contains $1.8 \cdot 10^{-21}$ mol glutamate, which is far too little to enable glutamate peaks. Therefore the buffer does not function properly in our current model.

We, therefore, experiment with different strengths of the EAAT currents. We differ the neuronal and the astrocytic EAAT permeability and measure the size of the glutamate dip. Figure 15 shows that weaker neuronal EAAT currents

result in smaller glutamate dips, while weaker astrocytic EAAT currents increase the glutamate dip. A low neuronal EAAT current means that the neuron can withdraw less glutamate from the ECS at a similar time, resulting in a smaller glutamate dip. On the other hand, a high astrocytic EAAT current results in a higher baseline of glutamate in the neuron in an unknown manner. The neuron can release this extra glutamate into the cleft and therefore needs to withdraw less glutamate from the ECS.

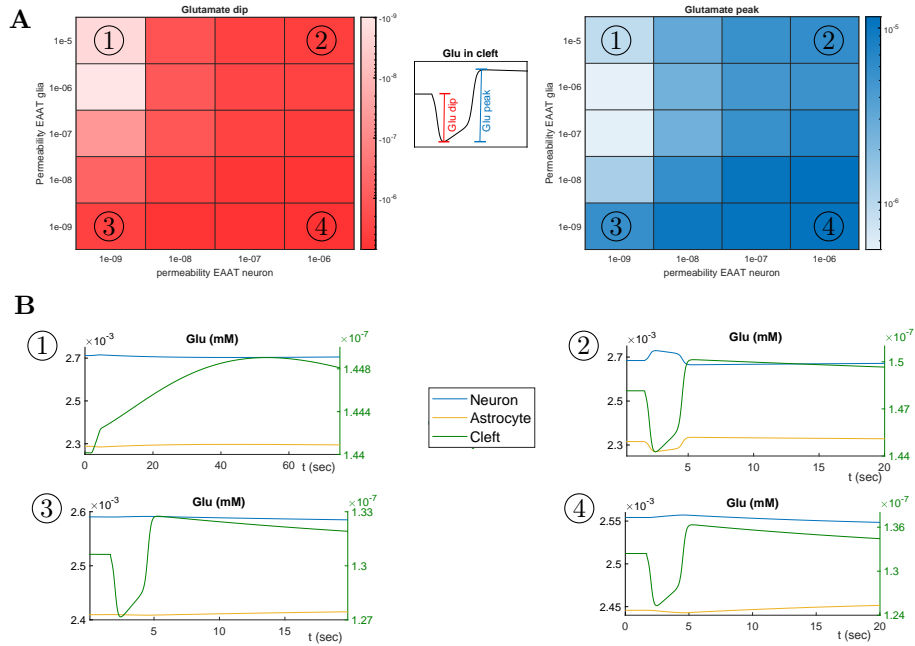


Figure 15: Glutamate dynamics after neuronal Ca^{2+} injection for different strengths of neuronal and astrocytic EAAT currents.

A: In red, we show the intensity of the glutamate dip, measured as the molar difference between baseline glutamate and minimum glutamate. In red we show the intensity of the glutamate peak (the molar difference between maximum and minimum glutamate). A weaker neuronal EAAT current can reduce the size of the glutamate dip, while a lower astrocytic EAAT permeability results in higher glutamate dips and higher glutamate peaks. The permeability of EAAT currents barely influences the amount of glutamate stored in the depot. B: We show the glutamate dynamics over time for the four situations in the corners of Figure A. A combination of low neuronal and high astrocytic EAAT permeability prevents the glutamate dip, but glutamate increase is slow and lasts 50 seconds after which glutamate concentrations return to baseline. All other simulations show similar dynamics, with a glutamate dip and a glutamate peak.

7 Discussion

In this research, we have conducted experiments with various types of stress and various ion injections to find possible causes for glutamate plumes. The results of all experiments are discussed below.

7.1 Glutamate release due to applied current and ED

An applied current can induce glutamate release through the onset of action potentials. Since experiments with TTX have shown that glutamate plumes do not depend on neuronal action potentials, an applied current is probably not responsible for glutamate plumes. Parker et al. [28] and Ziebarth and Reiner [49] showed that the amount of glutamate released during plumes is in the same order of magnitude as the amount of glutamate released during an action potential, indicating that we need glutamate release with an amplitude around $4.6 \cdot 10^{-5}$ mM/L to mimic glutamate plumes in our model.

Energy deprivation can cause neuronal action potentials that facilitate Ca^{2+} influx through voltage-gated Ca^{2+} channels. The released Ca^{2+} enables glutamate release into the cleft, causing a glutamate increase. Our simulation of energy deprivation during a blockade of the voltage-gated Na^+ current shows a similar amount of released glutamate, which indicates that the glutamate release during energy deprivation is mostly independent of neuronal action potentials. The glutamate release seems to be generated through neuronal Ca^{2+} -dependent synaptic glutamate release, similar as assumed for the glutamate plumes. However, glutamate release during energy deprivation of one second is significantly lower than that during a plume, while the onset time and recovery time are significantly longer. Although the glutamate release mechanism during energy deprivation shows similarities to the mechanisms leading to glutamate plumes, the duration, and intensity of glutamate release differ to the extent that we disqualify energy deprivation as a cause of the glutamate plumes.

7.2 Impact of neuronal glutamate transition rates

Our simulations indicate that glutamate transition rates do not influence glutamate release dynamics. The lack of change is unexpected since we expect that higher transition rates result in more glutamate release. The empty glutamate buffer could be responsible for the lack of change since it results in the absence of extra glutamate available for release.

7.3 Calcium induced glutamate release

Both neuronal and calcium injections can generate a glutamate peak with a duration similar to the duration of glutamate plumes. The calcium injection needs to be in the order of 1 mM to create these glutamate peaks, while the same amount of glutamate is released after an applied current where calcium

concentrations only increase by $3 \cdot 10^{-5}$. Simulations suggest that large Ca^{2+} injections are necessary to generate extracellular glutamate increase because the EAAT current is barely affected by a small calcium injection. We, therefore, hypothesize that a combination of increased cellular Ca^{2+} concentrations and decreased EAAT functionality are needed to generate glutamate plumes.

Furthermore, results indicate that glutamate peaks are more easily generated when astrocytic EAAT and NKA work at 50% than when these channels work at 100%. This is in line with the experiments of Ziebarth and Reiner [49] that show that the breakdown of glutamate clearance increases plume frequency, but does not directly indicate that plumes are induced by the breakdown of glutamate clearance.

7.4 Glutamate release due to temporal impairment of glutamate clearance

A temporal astrocytic EAAT block of 0.7 seconds with a fast onset and a slow recovery produces glutamate dynamics that are comparable to the glutamate plumes. This indicates that a temporal astrocytic EAAT block may be responsible for the glutamate plumes. A temporal block of 50% of both neuronal and astrocytic EAAT currents can also generate a glutamate peak with duration and amplitude similar to that of glutamate plumes. Therefore a temporal low functionality of both neuronal and astrocytic EAAT currents could also be responsible for glutamate plumes. We could not find any natural occurrences of temporal EAAT blocks in the literature. Therefore we suggest investigating temporal dysfunctioning EAAT protein in further research.

7.5 Cause of glutamate dip preceding glutamate peak

A shortcoming of the model causes a dip in glutamate concentrations before glutamate can be released. This problem is most likely caused by the lack of glutamate in the glutamate depot. Furthermore, we expect that the glutamate clearance rates are too high, and an adaption in EAAT permeability is necessary to solve this problem.

8 Limitations and further research

8.1 Limitations

As described in section 6.5, a dysfunctional glutamate buffer causes an unwanted dip in extracellular glutamate concentrations. To be able to simulate glutamate plumes, these dips should be resolved by adapting the EAAT permeability. Furthermore, The forward rate of glutamate going from the non-releasable pool to the depot should be adapted. This forward rate now depends on the concentration of glutamate in the depot, but the idea of a depot is that glutamate can

be stored there independent of the glutamate already present in the depot.

Another limitation of our model is the calcium response to depolarization. Blocking the voltage-gated sodium channel in our model represses action potentials during depolarization, but influences the calcium response only slightly. Jonas et al. [16] have shown that blocking the voltage-gated sodium channel with TTX in DRG somata reduces the electrically-evoked peak calcium response. Since our model does not reproduce this effect of TTX on the calcium response, we expect that the influence of the membrane potential on the permeability of the voltage-gated calcium channel is too small. We advise looking into the tuning of this permeability in further research.

8.2 Further research

We have several pieces of advice for further research, that can improve this research or that can give new insights into the mechanisms underlying glutamate plumes. This advice includes ideas for new simulations, researching the biological relevance of our results, and improving the used model.

First of all, we advise simulating a cell of an FHM2 mouse with various inputs. In our research, most experiments are done under baseline conditions. These experiments give insight into the effects of certain injections or stress factors, but Parker et al. [28] discovered that plumes are unlikely to arise under these baseline conditions. To simulate a cell of an FHM2 mouse, one should use a 50% functional EAAT and 50% functional NKA. The inputs should include injections with KCl and spreading depressions, since Parker et al. [28] hypothesize that stimuli that depolarize neuronal membrane potentials like a KCl injection and a spreading depression are sufficient to induce plumes.

Furthermore, we advise looking into the non-canonical opening of the voltage-gated calcium channels and non-canonical glutamate release. Research shows that calcium gates can open spontaneously in a stochastic manner [35], and that synaptic vesicle can spontaneously fuse and release a single packet of neurotransmitter [1]. Our results in section 6.3 suggest that the spontaneous inflow of calcium probably is not the trigger for glutamate plumes, but the spontaneous glutamate release, possibly in combination with spontaneous calcium inflow, may be responsible for glutamate plumes.

We also suggest looking into occurrences of spontaneous temporal dysfunction of EAAT proteins. Our simulations suggest that a temporal dysfunctioning of neuronal and astrocytic EAAT could be responsible for glutamate plumes, but we have not found literature on the natural occurrence of temporal EAAT malfunctioning.

To further improve the modelling of glutamate plumes, we also propose some alterations to the model. First, the glutamate dip described in section 6.5 should be solved by adapting EAAT permeability and the functioning of the glutamate buffer. Furthermore, we propose to include a calcium buffer in the astrocyte and/or neuron, a calcium-dependent glutamate cycle in the astrocyte, and receptors for extracellular glutamate that influence neuronal calcium availability. These extra mechanisms enable calcium-induced calcium release shown by de Pitta et al. [6]. The resulting neuronal calcium inflow may lead to glutamate plumes. A set-up for this addition is given in section C. Finally, we advise including diffusion in the model, either with surrounding cells or with a bath. The diffusion helps to clear glutamate from the cleft and may be responsible for the slow recovery of glutamate plumes.

9 Conclusion

Previous research suggests that glutamate plumes are a consequence of impaired astrocyte clearance in combination with synaptic calcium-dependent glutamate release [28]. Our results show that increased neuronal calcium on itself is unlikely to cause noteworthy glutamate release, but calcium increase during a temporal astrocytic EAAT block can result in plume-like glutamate release. Furthermore, we propose that stochastic temporal astrocytic EAAT malfunctioning can lead to glutamate plumes. We have further shown that energy deprivation does not result in plume-like glutamate release.

References

- [1] Laura C Andreae and Juan Burrone. The role of spontaneous neurotransmission in synapse and circuit development. *Journal of Neuroscience Research*, 96(3):354–359, 2018.
- [2] David Attwell and Simon B Laughlin. An energy budget for signaling in the grey matter of the brain. *Journal of Cerebral Blood Flow & Metabolism*, 21(10):1133–1145, 2001.
- [3] Laura Berliocchi, Daniele Bano, and Pierluigi Nicotera. Ca²⁺ signals and death programmes in neurons. *Philosophical Transactions of the Royal Society B: Biological Sciences*, 360(1464):2255–2258, 2005.
- [4] Dennis W Choi and Steven M Rothman. The role of glutamate neurotoxicity in hypoxic-ischemic neuronal death. *Annual review of neuroscience*, 13(1):171–182, 1990.
- [5] Niels C Danbolt. Glutamate uptake. *Progress in neurobiology*, 65(1):1–105, 2001.
- [6] Maurizio de Pittà, Vladislav Volman, Hugues Berry, and Eshel Ben-Jacob. A tale of two stories: Astrocyte regulation of synaptic depression and facilitation. *PLoS Computational Biology*, 7(12), 2011.
- [7] Jeffrey S Diamond and Craig E Jahr. Synaptically released glutamate does not overwhelm transporters on hippocampal astrocytes during high-frequency stimulation. *Journal of neurophysiology*, 83(5):2835–2843, 2000.
- [8] Xiao Xia Dong, Yan Wang, and Zheng Hong Qin. Molecular mechanisms of excitotoxicity and their relevance to pathogenesis of neurodegenerative diseases. *Acta Pharmacologica Sinica*, 30(4):379–387, 2009.
- [9] Marie Aimée Dronne, Jean Pierre Boissel, and Emmanuel Grenier. A mathematical model of ion movements in grey matter during a stroke. *Journal of Theoretical Biology*, 240(4):599–615, 2006.
- [10] Valery L Feigin, Michael Brainin, Bo Norrving, Sheila Martins, Ralph L Sacco, Werner Hacke, Marc Fisher, Jeyaraj Pandian, and Patrice Lindsay. World stroke organization (wso): global stroke fact sheet 2022. *International Journal of Stroke*, 17(1):18–29, 2022.
- [11] Piero Colli Franzone, Luca Franco Pavarino, and Simone Scacchi. *Mathematical cardiac electrophysiology*, volume 13. Springer, 2014.
- [12] Niklas J Gerkau, Cordula Rakers, Gabor C Petzold, and Christine R Rose. Differential effects of energy deprivation on intracellular sodium homeostasis in neurons and astrocytes. *Journal of neuroscience research*, 95(11):2275–2285, 2017.

- [13] Leif Hertz, Niklas J Gerkau, Junnan Xu, Simone Durry, Dan Song, Christine R Rose, and Liang Peng. Roles of astrocytic na^+ , k^+ -atpase and glycogenolysis for k^+ homeostasis in mammalian brain. *Journal of neuroscience research*, 93(7):1019–1030, 2015.
- [14] Jeannette Hofmeijer and Michel JAM van Putten. Ischemic cerebral damage: an appraisal of synaptic failure. *Stroke*, 43(2):607–615, 2012.
- [15] Niklas Hübel, Mahshid S. Hosseini-Zare, Jokūbas Žiburkus, and Ghanim Ullah. The role of glutamate in neuronal ion homeostasis: A case study of spreading depolarization. *PLoS Computational Biology*, 13(10):1–30, 2017.
- [16] Robin Jonas, Andreas Klusch, Martin Schmelz, Marlen Petersen, and Richard W Carr. Assessment of ttx-s and ttx-r action potential conduction along neurites of ngf and gdnf cultured porcine drg somata. *PLoS One*, 10(9):e0139107, 2015.
- [17] Anatoli Y Kabakov and Paul A Rosenberg. Evidence for change in current–flux coupling of glt1 at high glutamate concentrations in rat primary fore-brain neurons and glt1a-expressing cos-7 cells. *European Journal of Neuroscience*, 30(2):186–195, 2009.
- [18] Manu Kalia, Hil G.E. Meijer, Stephan A. van Gils, Michel J.A.M. van Putten, and Christine R. Rose. *Ion dynamics at the energy-deprived tripartite synapse*, volume 17. 2021.
- [19] Keetae Kim, Seok-Geun Lee, Timothy P Kegelman, Zhao-Zhong Su, Swadesh K Das, Rupesh Dash, Santanu Dasgupta, Paola M Barral, Michael Hedvat, Paul Diaz, et al. Role of excitatory amino acid transporter-2 (eaat2) and glutamate in neurodegeneration: opportunities for developing novel therapeutics. *Journal of cellular physiology*, 226(10):2484–2493, 2011.
- [20] Brian Roland Larsen, Rikke Holm, Bente Vilsen, and Nanna MacAulay. Glutamate transporter activity promotes enhanced na^+/k^+ -atpase-mediated extracellular k^+ management during neuronal activity. *The Journal of Physiology*, 594(22):6627–6641, 2016.
- [21] William Lee and Vladimir Parpura. *Protein Trafficking in Neurons*. Academic Press, 2006.
- [22] Chien-Liang Glenn Lin, Qiongman Kong, Gregory D Cuny, and Marcie A Glicksman. Glutamate transporter eaat2: a new target for the treatment of neurodegenerative diseases. *Future medicinal chemistry*, 4(13):1689–1700, 2012.
- [23] Eng H Lo, Turgay Dalkara, and Michael A Moskowitz. Mechanisms, challenges and opportunities in stroke. *Nature reviews neuroscience*, 4(5):399–414, 2003.

- [24] Anna R Malik and Thomas E Willnow. Excitatory amino acid transporters in physiology and disorders of the central nervous system. *International journal of molecular sciences*, 20(22):5671, 2019.
- [25] Aleksandra Mielnicka and Piotr Michaluk. Exocytosis in astrocytes. *Biomolecules*, 11(9), 2021.
- [26] Sandesh Mohan, Manindra Nath Tiwari, Yoav Biala, and Yoel Yaari. Regulation of neuronal na^+/k^+ -atpase by specific protein kinases and protein phosphatases. *Journal of Neuroscience*, 39(28):5440–5451, 2019.
- [27] Office of Communications NIH. What are the parts of the nervous system?, Jan 2018. retrieved 31-03-23.
- [28] Patrick D. Parker, Pratyush Suryavanshi, Marcello Melone, Punam A. Sawant-Pokam, Katelyn M. Reinhart, Dan Kaufmann, Jeremy J. Theriot, Arianna Pugliese, Fiorenzo Conti, C. William Shuttleworth, Daniela Pietrobon, and K. C. Brennan. Non-canonical glutamate signaling in a genetic model of migraine with aura. *Neuron*, 109(4):611–628, 2021.
- [29] Vladimir Parpura, Elizabeth S Fisher, James D Lechleiter, Arne Schousboe, Helle S Waagepetersen, Sylvain Brunet, Selva Baltan, and Alexei Verkhratsky. Glutamate and atp at the interface between signaling and metabolism in astroglia: examples from pathology. *Neurochemical research*, 42:19–34, 2017.
- [30] Stefan Passlick, Christine R Rose, Gabor C Petzold, and Christian Henneberger. Disruption of glutamate transport and homeostasis by acute metabolic stress. *Frontiers in Cellular Neuroscience*, 15:637784, 2021.
- [31] Allison R Peterson and Devin K Binder. Post-translational regulation of *glt-1* in neurological diseases and its potential as an effective therapeutic target. *Frontiers in molecular neuroscience*, 12:164, 2019.
- [32] James K. Peterson. *Ion Movement*, pages 97–147. Springer Singapore, Singapore, 2016.
- [33] AD Purdon, TA Rosenberger, HU Shetty, and SI Rapoport. Energy consumption by phospholipid metabolism in mammalian brain. *Neurochemical research*, 27(12):1641–1647, 2002.
- [34] MD Robert Teasell and Norhayati Hussein. Clinical consequences of stroke. *Evidence-Based Review of Stroke Rehabilitation. Ontario: Heart and Stroke Foundation and Canadian Stroke Network*, pages 1–30, 2016.
- [35] Ralf Schneggenburger and Christian Rosenmund. Molecular mechanisms governing ca^{2+} regulation of evoked and spontaneous release. *Nature Neuroscience*, 18(7):935–941, 2015.

- [36] Arne Schousboe. Glutamate neurotoxicity related to energy failure. *Handbook of Neurotoxicity*, pages 1–13, 2021.
- [37] Yasushi Shigeri, Rebecca P Seal, and Keiko Shimamoto. Molecular pharmacology of glutamate transporters, eaats and vgluts. *Brain Research Reviews*, 45(3):250–265, 2004.
- [38] Sade Spencer and Peter W. Kalivas. Glutamate transport: A new bench to bedside mechanism for treating drug abuse. *International Journal of Neuropsychopharmacology*, 20(10):797–812, 2017.
- [39] Thomas C. Südhof. The synaptic vesicle cycle. *Annual Review of Neuroscience*, 27:509–547, 2004.
- [40] Pawan Thapaliya, Nils Pape, Christine R Rose, and Ghanim Ullah. Modeling the heterogeneity of sodium and calcium homeostasis between cortical and hippocampal astrocytes and its impact on bioenergetics. *Frontiers in Cellular Neuroscience*, 2023.
- [41] Misha V. Tsodyks and Henry Markram. The neural code between neocortical pyramidal neurons depends on neurotransmitter release probability. *Proceedings of the National Academy of Sciences of the United States of America*, 94(2):719–723, 1997.
- [42] Michel J. A. M. van, Putten. *Dynamics of neural networks a mathematical and clinical approach*. Springer, 2020.
- [43] Alexander M. Walter, Paulo S. Pinheiro, Matthijs Verhage, and Jakob B. Sørensen. A Sequential Vesicle Pool Model with a Single Release Sensor and a Ca²⁺-Dependent Priming Catalyst Effectively Explains Ca²⁺-Dependent Properties of Neurosecretion. *PLoS Computational Biology*, 9(12), 2013.
- [44] Ji Wang, Fushun Wang, Dongmei Mai, and Shaogang Qu. Molecular mechanisms of glutamate toxicity in parkinson’s disease. *Frontiers in neuroscience*, 14:585584, 2020.
- [45] B Thomas William. Cerebrovascular disease. *Veterinary Clinics of North America: Small Animal Practice*, 26(4):925–943, 1996.
- [46] Alan Woodruff. What is a neuron?, Aug 2019. <https://qbi.uq.edu.au/brain/brain-anatomy/what-neuron>.
- [47] Bas-Jan Zandt, Bennie ten Haken, J Gert van Dijk, and Michel JAM van Putten. Neural dynamics during anoxia and the “wave of death”. *PLoS One*, 6(7):e22127, 2011.
- [48] Y. Zhou and N. C. Danbolt. Glutamate as a neurotransmitter in the healthy brain. *Journal of Neural Transmission*, 121(8):799–817, 2014.

- [49] Tim Ziebarth and Andreas Reiner. Faculty of Biology and Biotechnology
Glutamate dynamics during chemical ischemia : SF-iGluSnFR imaging
reveals “ plumes ” in cortical slices. Unpublished manuscript., 2021.

A Model formulation

The used model is described by Kalia et al. [18]. Below, we describe all differential equations present in the model.

A.1 Overview of the model notations

The model describes the dynamics of molar amounts of the ions Na^+ , K^+ , Cl^- , Ca^{2+} and glutamate. The model contains six compartments: the neuron (n), presynaptic terminal (ps), astrocyte (a), extracellular space (e) and cleft (c). The molar amount of ion X in compartment i is defined as N_X^i , and the volume of compartment i is given by W_i . The concentration of ion X in compartment i is defined as $[X]_i$. To describe the dynamics, we use currents and fluxes $I_Y^{X,i}$, the current of ion X in compartment I through the channel Y . We take the leak and gated currents into account, and the EAAT-, NCX-, NKA-, KCl-, NKCC1- and Kir- currents.

A summary of the notations is given in table 2.

Notation	Description
N_X^i	Molar amount of ion X in compartment i .
$[X]_i$	Concentration of ion X in compartment i .
W_i	Volume of compartment i .
$I_Y^{X,i}$	Current/flux contribution of ion channel/transporter Y with respect to ion X in compartment i .
V_i	Membrane potential with respect to compartment i .
z_X	Valence of ion X .
$P_Y^{X,i}$	Permeability/strength/conductance of ion channel/transporter Y with respect to ion X in compartment i .
Choices for i, X, Y	
i	n (neuronal soma), a (astrocyte soma), e (extracellular space), ps (presynaptic terminal), pap (perisynaptic astrocyte process) or c (cleft).
X	Na^+ , K^+ , Cl^- , Ca^{2+} , or Glu (glutamate).
Y	EAAT, NCX, NKA, KCl, NKCC1, Kir, G (gated) or L (Leak).

Table 2: Notation used in the model equations

Ion concentrations and membrane potentials

The model determines ion concentrations in different compartments. We assume that Na^+ , K^+ , and Cl^- concentrations are the same in the somatic and synaptic

compartments, which gives us

$$[X]_n = [X]_{ps}, \quad (20)$$

$$[X]_a = [X]_{pap}, \quad (21)$$

$$[X]_e = [X]_c, \quad X \in (\text{Na}^+, \text{K}^+, \text{Cl}^-) \quad (22)$$

We assume that the volumes W_{ps} , W_c , and W_{pap} are constant, and we assume that all glutamate is contained in the synaptic compartments so

$$[X]_n = [X]_{ps}, \quad (23)$$

$$[X]_a = [X]_{pap}, \quad (24)$$

$$[X]_e = [X]_c, \quad X \in (\text{Ca}^{2+}, \text{Glu}) \quad (25)$$

When we know the molar amounts of the ions and glutamate, we can calculate the membrane potential as

$$V_i = \frac{F}{C_i} \sum_X z_X N_X^i, \quad (26)$$

where $i = \{n, a\}$. Here, F is Faraday's constant, C is the membrane capacitance, and z_X is the valance of ion X .

A.2 Neuronal dynamics

We use the following currents and fluxes to describe neuronal somatic dynamics:

1. voltage-gated Na^+ , K^+ , Cl^- and Ca^{2+} channels
2. leak currents
3. Na^+/K^+ -ATPase (NKA),
4. K^+/Cl^- -cotransporter (KCC)
5. $\text{Na}^+/\text{Ca}^{2+}$ -exchanger (NCX)
6. Excitatory Amino Acid Transporter (EAAT)

A.2.1 Voltage gated currents and leak currents

We use the Goldman-Hodgkin-Katz (GHK) currents to describe the voltage-gated and leak currents. The voltage gated currents are described as

$$I_G^{\text{Na}^+,n} = P_G^{\text{Na}^+,n} m^3 h \text{GHK}(V_n, [\text{Na}^+]_n, [\text{Na}^+]_e) \quad (27)$$

$$I_G^{\text{K}^+,n} = P_G^{\text{K}^+,n} m^4 \text{GHK}(V_n, [\text{K}^+]_n, [\text{K}^+]_e) \quad (28)$$

$$I_G^{\text{Ca}^{2+},n} = 4P_G^{\text{Ca}^{2+},n} m^2 h \text{GHK}(V_n, [\text{Ca}^{2+}]_n, [\text{Ca}^{2+}]_e) \quad (29)$$

$$I_G^{\text{Cl}^-,n} = \frac{P_G^{\text{Cl}^-,n}}{1 + \exp(-(V_n + 10)/10)} \text{GHK}(V_n, [\text{Cl}^-]_n, [\text{Cl}^-]_e). \quad (30)$$

The neuronal leak current for ion X is dependent on the membrane potential and the intracellular and extracellular concentration of X as

$$I_L^{X,n} = P_L^{X,n} GHK(V_n, [X]_n, [X]_e). \quad (31)$$

The function $GHK(V_y, [X]_y, [X]_e)$ is defined as

$$GHK(V_y, [X]_y, [X]_e) = \frac{z_X^2 F^2 V_y}{RT} \frac{[X]_y - [X]_e \exp\left(\frac{-FV_y z_X}{RT}\right)}{1 - \exp\left(\frac{-FV_y z_X}{RT}\right)}. \quad (32)$$

The values m , h , and n represent the opening and closing of the gates and are given by

$$\frac{d}{dt}q = \alpha_q(1 - q) - \beta_q q \quad (33)$$

for $q \in (m, h, n)$. α_q and β_q are voltage-dependent functions given by

$$\alpha_m = \frac{0.32(V + 52)}{1 - \exp(-(V + 52)/4)}, \quad \beta_m = \frac{0.28(V + 25)}{\exp((V + 25)/5) - 1}, \quad (34)$$

$$\alpha_h = 0.128 \exp(-(V + 53)/18), \quad \beta_h = \frac{4}{1 + \exp(-(V + 30)/5)}, \quad (35)$$

$$\alpha_n = \frac{0.016(V + 35)}{1 - \exp(-(V + 35)/5)}, \quad \beta_n = 0.25 \exp(-(V + 50)/40). \quad (36)$$

A.2.2 Active transport across neuronal membrane: NKA current

The NKA is located on the neuron's cell membrane and transports three Na^+ out of the cell in exchange for two K^+ by using one molecule of adenosine triphosphate (ATP). The currents of Na^+ and K^+ are modelled as

$$I_{\text{NKA}}^{\text{Na}^+,n} = 3I_{\text{NKA}}^n(t) \quad (37)$$

$$I_{\text{NKA}}^{\text{K}^+,n} = -2I_{\text{NKA}}^n(t) \quad (38)$$

where

$$I_{\text{NKA}}^n(t) = \left(\frac{I_{\text{NKA}}^{\text{max}}(t)}{100} \right) P_{\text{NKA}}^{\text{scale}} P_{\text{NKA}}^n g_{\text{NKA}} \frac{[\text{Na}^+]_n^{1.5}}{[\text{Na}^+]_n^{1.5} + (\alpha_{\text{NKA}}^n)^{1.5}} \frac{[\text{K}^+]_e}{[\text{K}^+]_e + (\beta_{\text{NKA}}^n)}. \quad (39)$$

and where $I_{\text{NKA}}^{\text{max}}$ is used to simulate energy deprivation for some time period as described in 5.1.3. The pump normal pump strength is given by P_{NKA}^n and can be adapted by changing $P_{\text{NKA}}^{\text{scale}}$. g_{NKA} is given by the voltage-dependent function

$$g_{\text{NKA}} = 1 + 0.1245 \exp(-0.1 \frac{FV_n}{RT}) + 0.0365\sigma \exp(-\frac{FV_n}{RT}) \quad (40)$$

with

$$\sigma = \frac{1}{7} \left(\exp\left(\frac{[\text{Na}^+]_e}{67.3}\right) - 1 \right). \quad (41)$$

A.2.3 Secondary active transport across neuronal membrane: KCC

The K^+ - Cl^- -cotransporter allows one Cl^- and one K^+ to leave the neuron. The Cl^- ions flow against their gradient and therefore this transporter provides a counter-current to the gated Cl^- channel. The flux is caused by an electrochemical gradient and is therefore modeled as the difference in Nernst potential between Cl^- and K^+ as

$$J_{KCl} = \frac{RT}{F} \ln \left(\frac{[K^+]_e [Cl^-]_e}{[K^+]_n [Cl^-]_n} \right). \quad (42)$$

The corresponding currents can be determined by multiplying the flux with Faraday's constant

$$I_{KCl}^{K^+,n} = F J_{KCl} \quad (43)$$

$$I_{KCl}^{Cl^-,n} = F J_{KCl}. \quad (44)$$

A.2.4 Secondary active transport: NCX

The Na^+ / Ca^{2+} -exchanger uses the electrochemical gradient to transport one Ca^{2+} from the synapse into the cleft in exchange for three Na^+ . The NCX current reverses when $[Na^+]_n$ increases above a threshold. We describe the NCX current by

$$I_{NCX}^i = P_{NCX}^i \left(\frac{[Na]_e^3}{\alpha_{Na^+}^3 + [Na^+]_e^3} \right) \left(\frac{[Cl^-]_c}{\alpha_{Ca^{2+}} + [Ca^{2+}]_c} \right) \times \quad (45)$$

$$\frac{\frac{[Na^+]_i^3}{[Na^+]_e^3} \exp\left(\frac{\eta F V_i}{RT}\right) - \frac{[Cl^-]_i}{[Cl^-]_c} \exp\left(\frac{(1-\eta) F V_i}{RT}\right)}{1 + k_{NCX} \exp\left(\frac{(\eta-1) F V_i}{RT}\right)}, \quad (46)$$

and the corresponding Na^+ and Ca^{2+} currents as

$$I_{NCX}^{Na^+,i} = 3 I_{NCX}^i, \quad (47)$$

$$I_{NCX}^{Ca^{2+},i} = -I_{NCX}^i. \quad (48)$$

A.2.5 Secondary active transport: EAAT

The Excitatory Amino Acid Transporter (EAAT) is responsible for the re-uptake of released glutamate. EAAT transports one glutamate, three Na^+ , and one K^+ into the cell in exchange for one H^+ . The flux through EAAT can be calculated as the difference in Nernst potentials by

$$J_{EAAT}^i = P_{EAAT}^i \frac{RT}{F} \ln \left(\frac{[Na^+]_e^3 [K^+]_i [H^+]_c [Glu]_c}{[Na^+]_i^3 [K^+]_e [H^+]_i [Glu]_i} \right). \quad (49)$$

The corresponding ion currents are

$$I_{\text{EAAT}}^{\text{Na}^+,i} = -3FJ_{\text{EAAT}}^i \quad (50)$$

$$I_{\text{EAAT}}^{\text{K}^+,i} = FJ_{\text{EAAT}}^i \quad (51)$$

$$I_{\text{EAAT}}^{\text{Glu},i} = FJ_{\text{EAAT}}^i, \quad (52)$$

and the ratio $\frac{[\text{H}^+]_c}{[\text{H}^+]_i}$ is kept constant.

A.3 Astrocytic dynamics

This section describes the incorporated channels and cotransporters that regulate astrocyte dynamics. We use the five different channels

1. Kir4.1 channel,
2. Na^+/K^+ -ATPase (NKA),
3. $\text{Na}^+/\text{K}^+/\text{Cl}^-$ -cotransporter (NKCC1),
4. $\text{Na}^+/\text{Ca}^{2+}$ -exchanger (NCX),
5. Excitatory Amino Acid Transporter (EAAT).
6. Leak currents

we will describe the Kir4.1 channel and the NKCC1 cotransporter below. The NKA current is already described for the neuron in section A.2.2 and can easily be adapted to the astrocyte by replacing every n in the equation by an a . Similarly the neuronal NCX current in section A.2.4, the neuronal EAAT current in section A.2.5, and the neuronal leak currents in section A.2.1 can be adapted to astrocytic currents by replacing the sub- en superscripts i by a .

A.3.1 Kir4.1 channel

The Kir4.1 channel on the astrocyte membrane transports K^+ from the extracellular space into the astrocyte, which helps to maintain the resting membrane potential. The current is given by

$$I_{\text{Kir}}^{\text{K}^+,a} = P_{\text{Kir}}m_{\infty} \frac{[\text{K}^+]_e}{[\text{K}^+]_e + 13} (V_a - E_K^a), \quad (53)$$

where

$$m_{\infty} = \left(2 + \exp \left(1.62 \frac{F}{RT} (V_a - E_K^a) \right) \right)^{-1}. \quad (54)$$

The reversal potential of potassium E_K^a is given by

$$E_K^a = \frac{RT}{F} \log \frac{[\text{K}^+]_e}{[\text{K}^+]_a}. \quad (55)$$

A.3.2 Secondary active transport: NKCC1

The Na^+ - K^+ - 2Cl^- -cotransporter (NKCC1) is located on the astrocyte membrane and transports one Na^+ , one K^+ and two Cl^- into the astrocyte. It is activated when extracellular K^+ levels are high. The astrocyte Cl^- regulation depends highly on NKCC1, and indirectly the NKCC1 plays a major role in astrocyte swelling. The flux through the NKCC1 channel is defined by the difference in Nernst potentials and is given by

$$J_{\text{NKCC1}}^a = P_{\text{NKCC1}}^a \frac{RT}{F} \log \left(\frac{[\text{Na}^+]_e [\text{K}^+]_e [\text{Cl}^-]_e^2}{[\text{Na}^+]_a [\text{K}^+]_a [\text{Cl}^-]_a^2} \right). \quad (56)$$

The Corresponding Na^+ , K^+ , and Cl^- currents are given by

$$I_{\text{NKCC1}}^{\text{Na}^+,a} = -F J_{\text{NKCC1}}^a, \quad (57)$$

$$I_{\text{NKCC1}}^{\text{K}^+,a} = -F J_{\text{NKCC1}}^a, \quad (58)$$

$$I_{\text{NKCC1}}^{\text{Cl}^-,a} = 2F J_{\text{NKCC1}}^a. \quad (59)$$

A.4 Glutamate cycle

The dynamics of glutamate in the model are more elaborate than other dynamics. We include the neuronal glutamate concentrations in specific stages. The stages are

- N_n : Non-releasable pool,
- R_n : Readily releasable pool,
- R_{1n} Vesicle bound 1Ca^{2+} ,
- R_{2n} Vesicle bound 2Ca^{2+} ,
- R_{3n} Vesicle bound 3Ca^{2+} ,
- F_n : Fused vesicle state,
- I_n : Inactive vesicle state,
- D_n : Vesicle depot.

The glutamate dynamics between these stages can be mathematically approximated by

$$\left\{ \begin{array}{l} \frac{d}{dt}N_{D_n} = \frac{1}{\tau_{rec,n}}N_{I_n}N_{D_n} - k_1N_{D_n} + k_{-1}N_{N_n}, \\ \frac{d}{dt}N_{N_n} = k_1N_{D_n} - (k_{-1} + k_2)N_{N_n} + k_{-2}N_{R_n}, \\ \frac{d}{dt}N_{R_n} = k_2N_{N_n} - (k_{-2} + 3k_3[Ca^{2+}]_n)N_{R_n} + k_{-3}N_{R_{1n}} \\ \frac{d}{dt}N_{R_{1n}} = 3k_3[Ca^{2+}]_nN_{R_n} - (k_{-3} + 2k_3[Ca^{2+}]_n)N_{R_{1n}} + 2k_{-3}N_{R_{2n}} \\ \frac{d}{dt}N_{R_{2n}} = 2k_3[Ca^{2+}]_nN_{R_{1n}} - (2k_{-3} + k_3[Ca^{2+}]_n)N_{R_{2n}} + 3k_{-3}N_{R_{3n}} \\ \frac{d}{dt}N_{R_{3n}} = k_3[Ca^{2+}]_nN_{R_{2n}} - (3k_{-3} + k_4)N_{R_{3n}} \\ \frac{d}{dt}N_{I_n} = -\frac{1}{\tau_{rec}}N_{I_n}N_{D_n} + \frac{1}{F}(I_{EAAT}^{Glu,n} + I_L^{Glu,n}) \end{array} \right. \quad (60)$$

The coefficients k_1 , k_2 and k_{-2} are given by

$$\begin{aligned} k_1 &= k_{1,max} \frac{[Ca^{2+}]_n}{[Ca^{2+}]_n + K_M} \\ k_2 &= k_{20} + g(Ca^{2+})k_{2cat} \\ k_{-2} &= k_{-20} + g(Ca^{2+})k_{-2cat} \end{aligned}$$

with

$$g(Ca^{2+}) = \frac{[Ca^{2+}]}{[Ca^{2+}] + K_{DV}}. \quad (61)$$

The glutamate concentrations in the neuron and in the cleft are defined as

$$[Glu]_n = [Glu]_{ps} = \frac{1}{W_{PreSyn}}N_{Glu}^n = \frac{1}{W_{PreSyn}}N_{I_n} \quad (62)$$

$$[Glu]_c = \frac{1}{W_c}N_{Glu}^c = \frac{1}{W_c}N_{F_n}. \quad (63)$$

The parameters for the glutamate dynamics are given in table 6. N_{F_n} is obtained from conservation laws to prevent numerical errors.

A.5 Volume dynamics

The model assumes that water movement between neuron, astrocyte and extracellular space depends linearly on the osmotic pressure gradient across the membrane. The volume of department $i \in \{n, a\}$ changes over time as

$$\frac{d}{dt}W_i = L_{H_2O}^i \Delta \pi_i \quad (64)$$

where $L_{\text{H}_2\text{O}}^i$ is the membrane water permeability and $\Delta\pi_i$ is the osmotic pressure gradient in department i given by

$$\Delta\pi_i = RT \sum_X ([X]_i - [X]_e), \quad (65)$$

for $X \in \{\text{Na}^+, \text{K}^+, \text{Cl}^-\}$.

A.6 Channel block

Apart from the NKA current, we can also block all modeled neuronal and astrocytic currents. When the current Y without a block is given by I_Y , we simulate a block of current Y by redefining

$$I_Y = I_Y \cdot \text{block}_Y \quad (66)$$

with

$$\text{block}_Y = \frac{1}{1 + \exp(100(t - t_{\text{start}Y}))} + \frac{1}{1 + \exp(-100(t - t_{\text{end}Y}))}. \quad (67)$$

The parameters $t_{\text{start}Y}$ and $t_{\text{end}Y}$ are the start and endtime of the block of current Y .

A.7 Model dynamics

Now that all individual currents are described, we can assemble all currents to obtain the set of differential equations

$$\left\{ \begin{array}{l}
\frac{d}{dt} N_{\text{Na}^+}^n = -\frac{1}{F} \left(I_G^{\text{Na}^+,n} + I_{\text{NK}A}^{\text{Na}^+,n} + I_{\text{E}A\text{A}T}^{\text{Na}^+,n} + I_{\text{N}C\text{X}}^{\text{Na}^+,n} + I_L^{\text{Na}^+,n} \right) + \frac{1}{F} I_{stim}(t), \\
\frac{d}{dt} N_{\text{K}^+}^n = -\frac{1}{F} \left(I_G^{\text{K}^+,n} + I_{\text{NK}A}^{\text{K}^+,n} + I_{\text{E}A\text{A}T}^{\text{K}^+,n} + I_{\text{K}Cl}^{\text{K}^+,n} + I_L^{\text{K}^+,n} \right), \\
\frac{d}{dt} N_{\text{Cl}^-}^n = \frac{1}{F} \left(I_G^{\text{Cl}^-,n} + I_{\text{K}Cl}^{\text{Cl}^-,n} + I_L^{\text{Cl}^-,n} \right), \\
\frac{d}{dt} N_{\text{Ca}^{2+}}^n = -\frac{1}{2F} \left(I_G^{\text{Ca}^{2+},n} + I_{\text{N}C\text{X}}^{\text{Ca}^{2+},n} + I_L^{\text{Ca}^{2+},n} \right), \\
\frac{d}{dt} N_{\text{Glu}}^n = \frac{1}{F} \left(I_{\text{E}A\text{A}T}^{\text{Glu},n} + I_L^{\text{Glu},n} \right), \\
\frac{d}{dt} N_{\text{Na}^+}^a = -\frac{1}{F} \left(I_{\text{NK}CC1}^{\text{Na}^+,a} + I_{\text{NK}A}^{\text{Na}^+,a} + I_{\text{E}A\text{A}T}^{\text{Na}^+,a} + I_{\text{N}C\text{X}}^{\text{Na}^+,a} + I_L^{\text{Na}^+,a} \right), \\
\frac{d}{dt} N_{\text{K}^+}^a = -\frac{1}{F} \left(I_{\text{NK}CC1}^{\text{K}^+,a} + I_{\text{NK}A}^{\text{K}^+,a} + I_{\text{E}A\text{A}T}^{\text{K}^+,a} + I_{\text{K}ir}^{\text{K}^+,a} + I_L^{\text{K}^+,a} \right), \\
\frac{d}{dt} N_{\text{Cl}^-}^a = \frac{1}{F} \left(I_{\text{NK}CC1}^{\text{Cl}^-,a} + I_L^{\text{Cl}^-,a} \right), \\
\frac{d}{dt} N_{\text{Ca}^{2+}}^a = -\frac{1}{2F} \left(I_{\text{N}C\text{X}}^{\text{Ca}^{2+},a} + I_L^{\text{Ca}^{2+},a} \right), \\
\frac{d}{dt} N_{\text{Glu}}^a = \frac{1}{F} \left(I_{\text{E}A\text{A}T}^{\text{Glu},a} + I_L^{\text{Glu},a} \right),
\end{array} \right. \quad (68)$$

Together with the equations for volume dynamics (equation (64)) and glutamate dynamics (equation (64)), this gives the basic model given by Kalia et al. [18].

A.8 Model constants and parameters

The tables 3 to 8 show the constants and parameters used in our model. All values are copied from Kalia et al [18].

Table 3: Model constants

Constant	Value	Description
C_n, C_a	20 pF	Membrane capacitance
F	96485.333 C/mol	Faraday's constant
R	8314.4598 C/(mol K)	universal gas constant
T	310K	Temperature
W_{ps}	10^{-3} [1000 μ m ³]	Fixed presynaptic terminal volume
W_c	10^{-3} [1000 μ m ³]	Fixed synaptic cleft volume
W_{pap}	10^{-3} [1000 μ m ³]	Fixed perisynaptic astrocyte process volume

Table 4: Model parameters for the neuronal compartment

Constant	Value	Description
$P_G^{\text{Na}^+,n}$	$8 \cdot 10^{-4}$ [1000 $\mu\text{m}^3/\text{ms}$]	Voltage-gated Na^+ channel permeability
$P_G^{\text{K}^+,n}$	$4 \cdot 10^{-4}$ [1000 $\mu\text{m}^3/\text{ms}$]	Voltage-gated K^+ channel permeability
$P_G^{\text{Cl}^-,n}$	$1.95 \cdot 10^{-5}$ [1000 $\mu\text{m}^3/\text{ms}$]	Voltage-gated Cl^- channel permeability
$P_G^{\text{Ca}^{2+},n}$	$1.5 \cdot 10^{-9}$ [1000 $\mu\text{m}^3/\text{ms}$]	Voltage-gated Ca^{2+} channel permeability
P_{NKA}^n	86.4 [pA]	Maximal NKA current
$\alpha_{NKA}^{\text{Na}^+}$	13 [mM]	NKA half-saturation concentration for intracellular Na^+
$\alpha_{NKA}^{\text{K}^+}$	0.2 [mM]	NKA half-saturation concentration for extracellular K^+
P_{KCl}^n	$1.3 \cdot 10^{-6}$ [fmol/(ms mV)]	KCl cotransporter strength
P_{NCX}^n	10.8 [pA]	NCX exchanger scaling factor
$\alpha_{NCX}^{\text{Na}^+}$	87.5 [mM]	NCX exchanger half-saturation concentration for Na^+
$\alpha_{NCX}^{\text{Ca}^{2+}}$	1.38 [mM]	NCX exchanger half-saturation concentration for Ca^{2+}
μ_{NCX}	0.35 [dimensionless]	NCX exchanger position of the energy barrier that controls voltage dependence of NCX current
k_{NCX}	0.1 [dimensionless]	NCX exchanger saturation factor at very negative potentials
P_{EAAT}^n	10^{-6} [fmol/(ms mV)]	Neuronal EAAT cotransporter strength
$\alpha_{H^+}^n$	0.66 [dimensionless]	Ratio of extracellular to intracellular proton concentration
$L_{H_2O}^n$	$2 \cdot 10^{-14}$ [1000 $\mu\text{m}^3 /(\text{mPa ms})$]	Neuronal membrane water permeability

Table 5: Model parameters for the astrocyte compartment

Constant	Value	Description
P_{Kir}^a	0.286102 [nS]	Kir4.1 conductance
P_{NKCC1}^a	$7.3215 \cdot 10^{-7}$ [fmol/(ms mV)]	NKCC1 cotransporter strength
P_{EAAT}^a	$2 \cdot 10^{-5}$ [fmol/(ms mV)]	Astrocyte EAAT cotransporter strength
P_{NKA}^a	86.4 [pA]	Maximal NKA current
$\alpha_{NKA}^{Na^+}$	13 [mM]	NKA half-saturation concentration for intracellular Na^+
$\alpha_{NKA}^{K^+}$	0.2 [mM]	NKA half-saturation concentration for extracellular K^+
P_{NCX}^a	5.7 [pA]	NCX exchanger scaling factor
$\alpha_{NCX}^{Na^+}$	87.5 [mM]	NCX exchanger half-saturation concentration for Na^+
$\alpha_{NCX}^{Ca^{2+}}$	1.38 [mM]	NCX exchanger half-saturation concentration for Ca^{2+}
μ_{NCX}	0.35 [dimensionless]	NCX exchanger position of the energy barrier that controls voltage dependence of NCX current
k_{NCX}	0.1 [dimensionless]	NCX exchanger saturation factor at very negative potentials
$\alpha_{H^+}^a$	0.66 [dimensionless]	Ratio of extracellular to intracellular proton concentration
$L_{H_2O}^a$	$2 \cdot 10^{-14}$ [1000 μm^3 / (mPa ms)]	Astrocyte membrane water permeability

Table 6: Model parameters for glutamate recycling

Constant	Value	Description
k_1^{max}	1 [1/ms]	Maximum forward reaction rate
K_M	$2.3 \cdot 10^{-3}$ [mM]	Ca ²⁺ half-saturation concentration for forward reaction rate (Depot to Non-Releasable pool)
K_{D_v}	$1 \cdot 10^{-4}$ [mM]	Half saturation concentration for forward reaction rate (Non-releasable pool to readily releasable pool)
k_{20}	$2.1 \cdot 10^{-5}$ [1/ms]	Uncatalysed forward reaction rate
$k_{2_{cat}}$	$2 \cdot 10^{-2}$ [1/ms]	Catalysed forward reaction rate
k_{-20}	$1.7 \cdot 10^{-5}$ [1/ms]	Uncatalysed backward reaction rate
k_{-1}	$5 \cdot 10^{-5}$ [1/ms]	backward reaction rate
k_3	4.4 [1/(mM ms)]	Forward reaction rate
k_{-3}	$5.6 \cdot 10^{-2}$ [1/ms]	Backward reaction rate
k_4	1.45 [1/ms]	Fusion rate
τ_{rec}	30 [ms/fmol]	Vesicle fusion factor

Table 7: Initial values for ion concentrations, gating variables, glutamate states, and volumes

Constant	Value	Description
V_i^0	-65.5 [mV]	Initial neuronal membrane potential
V_g^0	-80 [mV]	Initial astrocyte membrane potential
$[\text{Na}^+]_n^0$	13 [mM]	Initial neuronal sodium
$[\text{K}^+]_n^0$	145 [mM]	Initial neuronal potassium
$[\text{Cl}^-]_n^0$	7 [mM]	Initial neuronal chloride
$[\text{Ca}^{2+}]_n^0$	10^{-4} [mM]	Initial neuronal calcium
$[\text{Glu}]_n^0$	2.2385 [mM]	Initial neuronal glutamate
$[\text{Na}^+]_a^0$	13 [mM]	Initial astrocyte sodium
$[\text{K}^+]_a^0$	80 [mM]	Initial astrocyte potassium
$[\text{Cl}^-]_a^0$	35 [mM]	Initial astrocyte chloride
$[\text{Ca}^{2+}]_a^0$	10^{-4} [mM]	Initial astrocyte calcium
$[\text{Glu}]_a^0$	2 [mM]	Initial astrocyte glutamate
m_0	$1.33135 \cdot 10^{-2}$	Na^+ activation gating variable
h_0	0.987298	Na^+ inactivation gating variable
n_0	$2.96946 \cdot 10^{-3}$	K^+ activation gating variable
N_t^0	$2.238 \cdot 10^{-3}$ [fmol]	Initial molar amount of free glutamate in presynaptic terminal
N_D^0	$4.04605 \cdot 10^{-7}$ [fmol]	Initial molar amount of glutamate in the depot
N_N^0	$3.36567 \cdot 10^{-4}$ [fmol]	Initial molar amount of non releasable vesicular glutamate
N_R^0	$4.14849 \cdot 10^{-4}$ [fmol]	Initial molar amount of readily releasable vesicular glutamate (not yet binded to Ca^{2+})
$N_{R_1}^0$	$9.778061 \cdot 10^{-6}$ [fmol]	Initial molar amount of readily releasable vesicular glutamate (binded to one Ca^{2+} ion)
$N_{R_2}^0$	$7.655809 \cdot 10^{-8}$ [fmol]	Initial molar amount of readily releasable vesicular glutamate (binded to two Ca^{2+} ions)
$N_{R_3}^0$	$2.08192593 \cdot 10^{-11}$ [fmol]	Initial molar amount of readily releasable vesicular glutamate (binded to three Ca^{2+} ions)
W_n^0	2 [1000 μm^3]	Initial neuronal soma volume
W_a^0	2 [1000 μm^3]	Initial astrocyte soma volume

Table 8: Leak channel permeabilities, volumes and ion concentrations at $\alpha = 0.2$

Constant	Value	Description
$P_L^{\text{Na}^+,n}$	$1.706 \cdot 10^{-6}$ [1000 $\mu\text{m}^3/\text{ms}$]	Neuronal Na^+ leak channel permeability
$P_L^{\text{K}^+,n}$	$1.771 \cdot 10^{-5}$ [1000 $\mu\text{m}^3/\text{ms}$]	Neuronal K^+ leak channel permeability
$P_L^{\text{Cl}^-,n}$	$2.494 \cdot 10^{-6}$ [1000 $\mu\text{m}^3/\text{ms}$]	Neuronal Cl^- leak channel permeability
$P_L^{\text{Ca}^{2+},n}$	$1.649 \cdot 10^{-11}$ [1000 $\mu\text{m}^3/\text{ms}$]	Neuronal Ca^{2+} leak channel permeability
$P_L^{\text{Glu},n}$	$1.706 \cdot 10^{-6}$ [1000 $\mu\text{m}^3/\text{ms}$]	Neuronal Glutamate leak channel permeability
$P_L^{\text{Na}^+,a}$	$1.054 \cdot 10^{-7}$ [1000 $\mu\text{m}^3/\text{ms}$]	Astrocytic Na^+ leak channel permeability
$P_L^{\text{K}^+,a}$	$7.877 \cdot 10^{-5}$ [1000 $\mu\text{m}^3/\text{ms}$]	Astrocytic K^+ leak channel permeability
$P_L^{\text{Cl}^-,a}$	$4.38 \cdot 10^{-7}$ [1000 $\mu\text{m}^3/\text{ms}$]	Astrocytic Cl^- leak channel permeability
$P_L^{\text{Ca}^{2+},a}$	$3.022 \cdot 10^{-10}$ [1000 $\mu\text{m}^3/\text{ms}$]	Astrocytic Ca^{2+} leak channel permeability
$P_L^{\text{Glu},a}$	$2.891 \cdot 10^{-5}$ [1000 $\mu\text{m}^3/\text{ms}$]	Astrocytic glutamate leak channel permeability
W_e^0	0.925 [1000 μm^3]	Initial extracellular volume
N_{A-}^n	302.0105 [fmol]	Total amount of impermeant anions in the neuronal soma
N_{B+}^e	2.790 [fmol]	Total amount of cations in the extracellular space
N_{A-}^e	21.264 [fmol]	Total amount of impermeant anions in the extracellular space
N_{B+}^a	110.497 [fmol]	Total amount of cations in the astrocytic soma
N_{A-}^a	209.111 [fmol]	Total amount of impermeant anions in the astrocytic soma
C_{Na^+}	188.7 [fmol]	Total amount of Na^+ ions in the system
C_{K^+}	428.775 [fmol]	Total amount of K^+ ions in the system
C_{Cl^-}	198.375 [fmol]	Total amount of Cl^- ions in the system
$C_{\text{Ca}^{2+}}$	$1.8 \cdot 10^{-3}$ [fmol]	Total amount of Ca^{2+} ions in the system
C_{Glu}	$5 \cdot 10^{-3}$ [fmol]	Total amount of Glu ions in the system
W_{tot}	2.925 [1000 μm^3]	Total volume of the system

B Adaptations to the model and the code from Kalia et al.

The original code from Kalia et al. can be found at <https://github.com/mkalia94/TripartiteSynapse>. The model formulations can be found in the paper written by Kalia et al. [18]

B.1 Calcium current in the code

We have found a mistake in the python code of Kalia et al. in the formula for the neuronal voltage-gated calcium current. The current was given by

$$I_G^{\text{Ca}^{2+},n} = \frac{P_G^{\text{Ca}^{2+}} m^2 h^4 FV}{RT} \frac{(CaCi - CaCc)e^{-2FV/RT}}{1 - e^{-2FV/RT}} \quad (69)$$

instead of

$$I_G^{\text{Ca}^{2+},n} = \frac{P_G^{\text{Ca}^{2+}} m^2 h^4 F^2 V}{RT} \frac{(CaCi - CaCc)e^{-2FV/RT}}{1 - e^{-2FV/RT}}. \quad (70)$$

Note that the difference is the square above the constant F . We have adjusted the calcium permeability $P_G^{\text{Ca}^{2+}}$ to $1.5 \cdot 10^{-9}$ to make sure the gated calcium current remains in the same order of magnitude. We also adjust the strength of leak currents such that all dynamical equations are 0 in rest conditions:

$$\frac{d}{dt} N_{\text{Ca}^{2+}}^n = -\frac{1}{2F} (I_G^{\text{Ca}^{2+},n} + I_{\text{NCX}}^{\text{Ca}^{2+},n} + I_L^{\text{Ca}^{2+},n}) = 0. \quad (71)$$

We set the permeability of the calcium leak current $P_L^{\text{Ca}^{2+},n}$ such that this equation holds.

B.2 Formula for GHK current

The GHK current in the paper of Kalia et al. is given by,

$$\text{GHK}(V_y, [X]_y, [X]_e) = \frac{F^2 V_y}{RT z_X^2} \frac{[X]_y - [X]_e \exp\left(\frac{-FV_y}{RT z_X}\right)}{1 - \exp\left(\frac{-FV_y}{RT z_X}\right)} \quad (72)$$

(see equation (32)) but should be adapted to

$$\text{GHK}(V_y, [X]_y, [X]_e) = \frac{z_X^2 F^2 V_y}{RT} \frac{[X]_y - [X]_e \exp\left(\frac{-FV_y z_X}{RT}\right)}{1 - \exp\left(\frac{-FV_y z_X}{RT}\right)}. \quad (73)$$

This new formula is in line with the GHK current in literature [11, 32]. The GHK current was correctly implemented in python according to equation (73).

C Proposal of additional glutamate cycle in the astrocyte

The glutamate cycle described by Kalia et al. [18] covers the glutamate dynamics in the presynaptic terminal, but does not include glutamate dynamics in the postsynaptic astrocyte process. We expect that glutamate and calcium dynamics in the astrocyte have some influences on the dynamics in the presynaptic terminal. A numerical simulation by De Pitta et al. [6] shows that glutamate release by the astrocyte can either depress or facilitate synaptic neurotransmitter release. Furthermore, oscillations of Ca^{2+} in astrocytes can regulate presynaptic short-term depression or short-term facilitation (See Figure 2 by de Pitta et al. [6]). Additionally, experiments with TTX from Ziebarth and Reiner [49] show that the glutamate plumes are not induced by action potentials, which made us think about calcium-induced calcium release as the cause. We will add the glutamate dynamics in the postsynaptic astrocyte process to the model of Kalia et al. by relying heavily on the described processes by de Pitta [6], but also consulting other research. We will also include calcium dynamics and the influence of glutamate on these calcium dynamics.

C.0.1 Specification of processes

The model of Kalia et al. [18] has described various stages of glutamate in the neuron:

- D_n : Vesicle Depot in the presynaptic terminal
- N_n : Non-releasable pool in the presynaptic terminal
- R_n : Readily releasable pool in the presynaptic terminal
- R_{1n} : Vesicle binds to membrane using 1 Ca^{2+} in the presynaptic terminal (docking)
- R_{2n} : Vesicle binds to membrane using 2 Ca^{2+} in the presynaptic terminal (priming)
- R_{3n} : Vesicle binds to membrane using 3 Ca^{2+} in the presynaptic terminal (fusion-pore opening)
- I_n : Inactive vesicle state in the presynaptic terminal.

We assume that glutamate can have similar states in the astrocyte and therefore add the same states in the astrocyte. The transition between states is somewhat different, especially the fusion of the vesicle with the astrocytic cell membrane:

- D_a : Vesicle Depot in the perisynaptic astrocyte process
- N_a : Non-releasable pool in the perisynaptic astrocyte process

- R_a : Readily releasable pool in the perisynaptic astrocyte process
- R_{1a} : First step of vesicle binding to membrane in the perisynaptic astrocyte process (docking)
- R_{2a} : Second step of vesicle binding to membrane in the perisynaptic astrocyte process (priming)
- R_{3a} : Third step of vesicle binding to membrane in the perisynaptic astrocyte process (fusion-pore opening)
- I_a : Inactive vesicle state in the perisynaptic astrocyte process

When glutamate is released from the neuron, the glutamate enters the synaptic cleft. De Pitta et al.[6] describes that the astrocyte releases glutamate into an extra synaptic cleft. Therefore we add these two states to the states of glutamate.

- ESC (Extra synaptic cleft): Vesicle is fused with the perisynaptic astrocyte process membrane, and glutamate is in the extra synaptic cleft.
- SC (Synaptic cleft): Vesicle is fused with the presynaptic terminal membrane and glutamate is in the synaptic cleft.

Figure 16 shows an overview of the transition between these states. The relation between neuronal glutamate states is similar as described by Kalia et al. [18]. Astrocytic states have similar transitions as the neuron, with an adaptation on the calcium dependence and different reaction rates. The relations with the synaptic cleft and the extra-synaptic cleft are taken from Figure 1 of the paper by de Pitta et al. [6].

The binding of a vesicle to a membrane usually happens in four steps: docking, priming, fusion-pore opening, and full fusion [25]. In the neuron, the four steps all require calcium. In the astrocyte, the docking and priming do not require calcium ions, but the opening of the fusion pore requires calcium ions, similar to the neuron. The full fusion in the astrocyte is an ATP-dependent process.

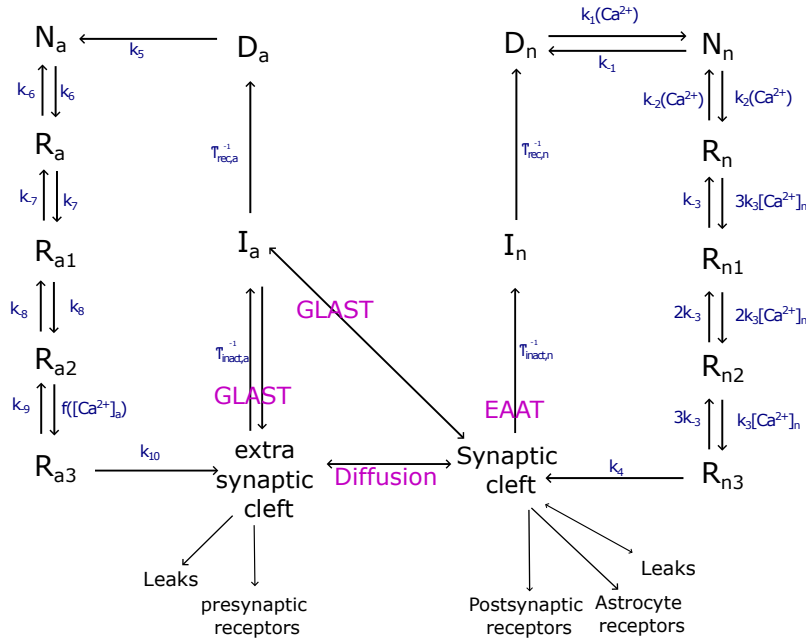


Figure 16: Glutamate cycle in both the neuron and the astrocyte. Glutamate in the presynaptic terminal is stored in Non releasable vesicles (N_n). These vesicles move closer to the cell membrane and fuse together with the cell membrane through four calcium dependent processes (R_n , R_{n1} , R_{n2} , R_{n3}). When the vesicle is fully fused (F_n), the glutamate from this vesicle is released into the synaptic cleft [18, 41, 43, 39]. Here it can bind to postsynaptic receptors and astrocyte receptors. It is important that the free glutamate molecules are taken up in fast processes, since excessive activation of postsynaptic receptors may excite nerve cells to death in a process called excitotoxicity [48, 3]. This uptake is partially done by EAATs and leak channels on the membrane of the presynaptic terminal (I_n)[18], after which glutamate is taken up from vesicles from the depot (D) to again form non releasable vesicles (N_n)[39]. The astrocyte also takes up glutamate from the synaptic cleft through EAAT/GLAST (I_A) [6, 38]. Vesicles from a depot in the astrocyte (D_A) take up the glutamate and form non releasable vesicles in the astrocyte. The vesicles in the astrocyte travel to the cell membrane [21], and merge with the cell membrane under influence of calcium. This happens through 4 stages: R_a , R_{a1} , R_{a2} , R_{a3} . The step from R_{a2} , to R_{a3} is the only calcium dependent step in this process [25]. Once the vesicle is fused with the cell membrane (F_A), glutamate is released into an extra synaptic space [6], where it can bind to presynaptic receptors.

The relations between states can be described by a set of differential equations. The neuronal differential equations are obtained from [41, 43], and have already been combined in [18].

$$\left\{ \begin{array}{l} \frac{d}{dt} N_{D_n} = \frac{1}{\tau_{rec,n}} N_{I_n} N_{D_n} - k_1 N_{D_n} + k_{-1} N_{N_n}, \\ \frac{d}{dt} N_{N_n} = k_1 N_{D_n} - (k_{-1} + k_2) N_{N_n} + k_{-2} N_{R_n}, \\ \frac{d}{dt} N_{R_n} = k_2 N_{N_n} - (k_{-2} + 3k_3[Ca^{2+}]_n) N_{R_n} + k_{-3} N_{R_{1n}}, \\ \frac{d}{dt} N_{R_{1n}} = 3k_3[Ca^{2+}]_n N_{R_n} - (k_{-3} + 2k_3[Ca^{2+}]_n) N_{R_{1n}} + 2k_{-3} N_{R_{2n}}, \\ \frac{d}{dt} N_{R_{2n}} = 2k_3[Ca^{2+}]_n N_{R_{1n}} - (2k_{-3} + k_3[Ca^{2+}]_n) N_{R_{2n}} + 3k_{-3} N_{R_{3n}}, \\ \frac{d}{dt} N_{R_{3n}} = k_3[Ca^{2+}]_n N_{R_{2n}} - (3k_{-3} + k_4) N_{R_{3n}}, \\ \frac{d}{dt} N_{I_n} = -\frac{1}{\tau_{rec}} N_{I_n} N_{D_n} + \frac{1}{F} (I_{EAAT}^{Glu,n} + I_L^{Glu,n}). \end{array} \right. \quad (74)$$

The equations in the astrocyte have slightly different processes, but the overall cycle is similar. The main difference is that the steps from R_a to R_1 and from R_1 to R_2 are not calcium-dependent. The transition between the states can be described by the differential equations:

$$\left\{ \begin{array}{l} \frac{d}{dt} N_{D_a} = \frac{1}{\tau_{rec,a}} N_{I_a} N_{D_a} - k_1 N_{D_a}, \\ \frac{d}{dt} N_{N_a} = k_5 N_{D_a} - k_6 N_{N_a} + k_{-6} N_{R_a}, \\ \frac{d}{dt} N_{R_a} = k_6 N_{N_a} - (k_{-6} + k_7) N_{R_a} + k_{-7} N_{R_{1a}}, \\ \frac{d}{dt} N_{R_{1a}} = k_7 N_{R_a} - (k_{-7} + k_8) N_{R_{1a}} + k_{-8} N_{R_{2a}}, \\ \frac{d}{dt} N_{R_{2a}} = 2k_8 N_{R_{1a}} - (k_{-8} + f([Ca^{2+}]_a)) N_{R_{2a}} + k_{-9} N_{R_{3a}}, \\ \frac{d}{dt} N_{R_{3a}} = f([Ca^{2+}]_a) N_{R_{2a}} - (k_{-9} + k_{10}) N_{R_{3a}}, \\ \frac{d}{dt} N_{ESC} = k_{10} N_{R_{3a}} - \frac{1}{F} (I_{Glast}^{Glu,a} + I_L^{Glu,a}) + I_{diffusion}^{Glu}, \\ \frac{d}{dt} N_{I_a} = -\frac{1}{\tau_{rec_a}} N_{I_a} N_{D_a} + \frac{1}{F} (I_{GLAST}^{Glu,a} + I_{GLAST}^{Glu,n} + I_L^{Glu,a}), \end{array} \right. \quad (75)$$

The expression for N_{ESC} is derived from conservation laws. The equations for the currents through the different gates will be calculated similarly as the current through the EAAT described in appendix A.2.5.

The glutamate in the extrasynaptic cleft will activate presynaptic receptors mGluRs and NMDAR [6]). These will modulate (de Pittas picture shows inhibition, but there are more processes according to the caption) the amount of calcium available for the calcium dependent fusion processes in the presynaptic terminal. Glutamate in the synaptic cleft can activate postsynaptic receptors, which trigger Ca^{2+} release from astrocytic endoplasmic reticulum. A recent paper by Thapaliya et al. [40] can be used to obtain formulas for the calcium dynamics.